DEVELOPMENT OF LSF-BASED DUAL-PHASE CATHODES FOR INTERMEDIATE TEMPERATURE SOLID OXIDE FUEL CELLS

A THESIS SUBMITTED TO
THE GRADUATE SCHOOL OF NATURAL AND APPLIED SCIENCES
OF
MIDDLE EAST TECHNICAL UNIVERSITY

BY

RAMIN BABAZADEH DIZAJ

IN PARTIAL FULFILLMENT OF THE REQUIREMENTS
FOR
THE DEGREE OF MASTER OF SCIENCE
IN
METALLURGICAL AND MATERIALS ENGINEERING

DECEMBER 2022

Approval of the thesis:

DEVELOPMENT OF LSF-BASED DUAL-PHASE CATHODES FOR INTERMEDIATE TEMPERATURE SOLID OXIDE FUEL CELLS

submitted by **RAMIN BABAZADEH DIZAJ** in partial fulfillment of the requirements for the degree of **Master of Science in Metallurgical and Materials Engineering, Middle East Technical University** by,

Prof. Dr. Halil Kalıpçılar
Dean, Graduate School of **Natural and Applied Sciences** _____

Prof. Dr. Ali Kalkanlı
Head of the Department, **Met. and Mat. Eng. METU** _____

Prof. Dr. Yunus Eren Kalay
Supervisor, **Met. and Mat. Eng. METU** _____

Prof. Dr. Tayfur Öztürk
Co-Supervisor, **Met. and Mat. Eng. METU** _____

Examining Committee Members:

Prof. Dr. Kadri Aydınol
Metallurgical and Materials Eng., METU _____

Prof. Dr. Yunus Eren Kalay
Metallurgical and Materials Eng., METU _____

Prof. Dr. Tayfur Öztürk
Metallurgical and Materials Eng., METU _____

Prof. Dr. Çiğdem Toparlı
Metallurgical and Materials Eng., METU _____

Assoc. Prof. Dr. Hasan Akyıldız
Metallurgical and Materials Eng., Konya Technical University _____

Date: ...

I hereby declare that all information in this document has been obtained and presented in accordance with academic rules and ethical conduct. I also declare that, as required by these rules and conduct, I have fully cited and referenced all material and results that are not original to this work.

Name Last name : Ramin Babazadeh Dizaj

Signature :

ABSTRACT

DEVELOPMENT OF LSF-BASED DUAL-PHASE CATHODES FOR INTERMEDIATE TEMPERATURE SOLID OXIDE FUEL CELLS

Babazadeh Dizaj, Ramin
Master of Science, Metallurgical and Materials Engineering
Supervisor: Prof. Dr. Yunus Eren Kalay
Co-Supervisor: Prof. Dr. Tayfur Öztürk

December 2022, 54 pages

In this thesis, a study was carried out on LSM-LSF composite cathodes for IT-solid oxide fuel cells. The study follows the previous work carried out on LSC113-LSC214 dual-phase and LSM/LSF/ScSZ composite cathodes, both developed for IT-SOFCs.

The study involved the synthesis of active material, namely $(La_{0.5}Sr_{0.5})MnO_{3-\delta}$ (LSM), $(La_{0.8}Sr_{0.2})FeO_{3-\delta}$ (LSF), and $Sc_{0.15}Zr_{0.85}O_{2-\delta}$ (ScSZ) via Pechini method. Symmetric cells were fabricated, and cathodes were characterized electrochemically via EIS measurements. For this purpose, ScSZ electrolyte discs were produced via a tape-casting method. The discs were used as the substrates on which cathodes of the same composition were deposited via sputter deposition on both sides of the electrolyte using sputter targets produced from the synthesized powders.

LSM/LSF composite cathodes with different compositions were obtained via combinatorial sputter deposition yielding composite cathodes with composition ranging from LSM: LSF=7:93 to LSM: LSF=62:38. The symmetric cells with these cathodes were electrochemically characterized for temperatures ranging from 600 to 800°C with 50°C intervals. The study has shown that the area-specific resistance

values were, in general, less than ASR=0.3 ohm.cm^2 at 800°C for all compositions The lowest temperature for which the benchmark value of ASR= 0.15 ohm.cm^2 was obtained was 780°C. This was obtained for $LSM_{42}LSF_{58}$ where the constituent oxides had nearly equal proportions.

Keywords: SOFC, Cathode, LSM, LSF, Magnetron sputtering.

ÖZ

LSF ESASLI ÇİFT FAZLI KATODLARIN ORTA SICAKLIK KATI OKSİT YAKIT PİLLERİ İÇİN GELİŞTİRİLMESİ

Babazadeh Dizaj, Ramin
Yüksek Lisans, Metalurji ve Malzeme Mühendisliği
Tez Yöneticisi: Prof. Dr. Yunus Eren Kalay
Ortak Tez Yöneticisi: Prof. Dr. Tayfur Öztürk

Aralık 2022, 54 sayfa

Sıçratma-çöktürme yöntemi ile sentezlenen $(La,Sr)CoO_3$-$(La,Sr)_2CoO_4$ amorf katotları üzerinde yapılan öncül bir çalışmanın ardından, bu tezde $(La,Sr)FeO_x$ (LSF)-$(La,Sr)MnO_3$ (LSM) kompozit katotları konu alan benzer bir çalışma yapılmıştır. Bu tez LSM/LSF/ScSZ üçlü katod sisteminde konu alan kapsamlı bir araştırmayı esas almakta ve bu çalışmanın tespitlerinden hareketle LSM-LSF ikili sistemine odaklanmaktadır.

Bu amaçla LSM ve LSF hedef diskleri kullanılarak kombinatoryal geometride 6 katottan oluşan bir set sıçratma-çöktürme yöntemi ile katodlar geliştirilmiştir. Katotların elektrokimyasal performansı simetrik hücre kullanılarak ölçülmüştür. Bu amaçla elektrolit olarak ScSZ diskler üretilmiş ve her iki yüzeyleri katodla kaplanmıştır. EIS Testleri, 50°C aralığında 600°C'den başlanarak gerçekleştirilmiş ve alan spesifik direnç değerinin (ASD) $\leq$ 0,15 ohm.cm^2 olduğu sıcaklık tespit edilmiştir. Yapılan çalışma orta kompozisyonlarda amaçlanan ASD değerinin daha düşük sıcaklıklarda oluştuğunu göstermiş ve en düşük sıcaklık $LSM_{42}LSF_{58}$ kompozisiyonunda 780°C de elde edilmiştir.

Anahtar Kelimeler: Katı Oksit Yakıt Pilleri (KOYP), Katot, LSM, LSF, Çoklu yaklaşımla malzeme geliştirme, Sıçratma-çöktürme ile ince film oluşturma.

Dedicated to my Kind-Hearted Family

ACKNOWLEDGMENTS

There is no doubt that this study would not be possible to be done without the help and assistance of my family, friends, and colleagues. Although these are only the words versus their kindness, I would like to appreciate them.

I would like to thank the precious guidance and support of my supervisor Prof. Dr. Tayfur Öztürk. His valuable advice always paved the way for me to do this study and also changed my academic path.

I am thankful to all who helped me in the Metallurgical and Materials Eng. Dept. and specifically my lab mates in the center of Materials for Energy Storage and Conversion Devices: N. Özgür Darıcıoğlu, Fahrettin Kılıç, Pelin Livan, Aylin Elçi, Yiğit Akbaş, H. Aybike Can and H. Eda Aysal.

Most importantly, I would like to thank my parents, Elyas Babazadeh Dizaj and Fariba Farzamnia, and also my brother Shahin Babazadeh Dizaj. I know that words are not enough to thank them, but this is the only way of expressing myself. Their support, even at rough times of my life economically and emotionally, made me possible to continue on my own goals.

Last but not least, I would Like to thank my lovely girlfriend, Nastaran Sabahi, who helped me whenever I needed.

Also, I would like to thank the Scientific and Technological Research Council of Turkey (TUBITAK) for their financial support under Grant No. 217M628.

TABLE OF CONTENTS

LIST OF TABLES

TABLES

LIST OF FIGURES

FIGURES

LIST OF ABBREVIATIONS

ABBREVIATIONS

Area Specific Resistance (ASR)

$Ba_{0.5}Sr_{0.5}Co_{0.8}Fe_{0.2}O_{3-\delta}$ (BSCF)

Calcia-stabilized zirconia (CSZ)

Gadolinium doped Ceria (GDC) or (CGO)

10% Gd doped-CeO_2 (GDC-10)

High Entropy Perovskites (HEP)

Intermediate Temperature Solid Oxide Fuel Cell (IT-SOFC)

$(La,Sr)CoO_3$ (LSC-113)

$(La,Sr)_2CoO_4$ (LSC-214)

$La_xSr_{1-x}Co_yFe_{1-y}O_3$ (LSCF)

$(La,Sr)FeO_x$ (LSF)

$(La,Sr)MnO_3$ (LSM)

Manganese-stabilized zirconia (MSZ)

Proton-conducting SOFC (H-SOFC)

Solid Oxide Fuel Cell (SOFC)

$Sc_{0.15}Zr_{0.85}O_{2-\delta}$ (ScSZ)

Samarium doped Ceria (SDC)

Strontium doped Samarium Manganite (SSM)

Triple Phase Boundary (TPB)

$(ZrO2)_{1-x}(Y_2O_3)_x$ (YSZ)

CHAPTER 1

INTRODUCTION

It is well-known fact that clean energy is essential for a sustainable ecosystem. One of the most prominent strategies in clean energy is to use electrochemical conversion devices. Fuel cells are one of the best devices of this kind. Although the function of these conversion devices looks like batteries, they can produce the needed energy as long as the fuel is supplied to the device.

There are a variety of fuel cells, e.g., alkaline fuel cells (AFC), Molten carbonate fuel cells (MCFC), Polymer electrolyte membrane fuel cells (PEMFC), Solid oxide fuel cells (SOFC), etc. (Guangul et al. 2020). Of these, SOFCs and PEMFCs are the most prominent and have attracted considerable attention. PEM fuel cells are attractive due to their applications for portable devices that operate close to ambient temperatures and make use of pure hydrogen as fuel. SOFC operates at elevated temperatures and has improved energy efficiency, and more importantly, has fuel flexibility, i.e., it operates on hydrogen as well as on hydrocarbons.

The basic difference between PEM fuel cells and SOFC is related to their electrolyte. In the PEM fuel cell, the electrolyte is generally Nafion (Bi et al. 2007). The operation of a fuel cell relies on the diffusion of protons to the cathode side, where it reacts with oxygen. In the case of SOFC, the electrolyte is an oxide with high ionic conductivity through which the oxygen reduced at the cathode diffuses to the anode side, where the reaction takes place with hydrogen.

In theory, the structure of SOFC is pretty straightforward. They have dense electrolytes and two electrodes on each side. Oxygen molecules from the air enter the system through the cathode side via an oxygen reduction reaction (ORR):

$$\tfrac{1}{2}\, O_2\,(g) + 2e^- \rightarrow O^{2-}$$

It is, therefore, a necessity for the cathode layer to have an acceptable oxygen reduction rate, plus it must possess sufficient electronic conductivity so that it can supply electrons to the reaction. The ionized oxygen diffuses through the electrolyte as a result of the concentration gradient and reaches the anode side.

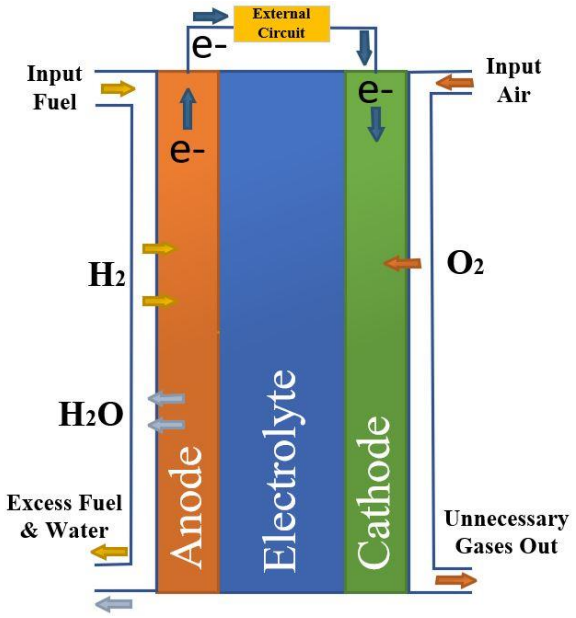

Figure 1.1. Schematic representation of SOFC (adapted from Habibi et al. 2019).

Electrolyte should be ion conductors to let the oxygen ions pass to the anode side, but they should be electronic insulators to impede the electron movement across the electrolyte.

The anode is the layer through which hydrogen (or other hydrocarbons) are supplied to the SOFCs. The reaction takes place in anode (taking hydrogen into account only).

$$H_2 + O^{2-} \longrightarrow H_2O + 2e^-$$

Thus, the overall reaction in the fuel cell is:

$$H_2 + O \;=\; H_2O$$

Therefore, anode should possess both protonic and electronic conductivity. In addition, anode should be porous so that the gaseous fuel can be fed to penetrate its structure.

SOFCs, with their basic structure given above, traditionally operate at elevated temperatures, e.g., 800-1000°C (Yang et al. 2020). The cathode is typically LSM, electrolyte is YSZ, and the anode is Ni-YSZ. The biggest drawback of this type of fuel cell are a long start-up and cool-down time, material degradation mechanically and chemically, sealant problems etc.

Attempts to reduce the operating temperature of SOFCs has been the subject of many recent studies. The main obstacle in lowering the operating temperature of SOFC is the sluggish rate of oxygen reduction reaction at reduced temperatures.

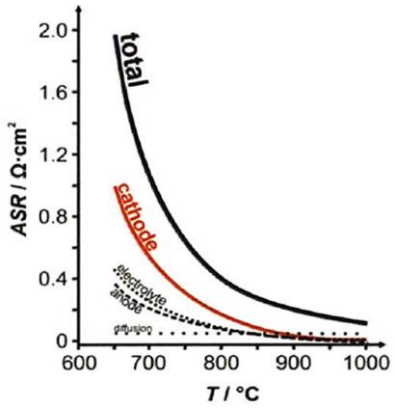

Figure 1.2. ASR values vs. temperature in SOFC. (Sase et al. 2008)

Development of MIEC cathodes in this respect provided a breakthrough where acceptable rate of oxygen reduction reaction was achieved at intermediate temperatures. Cathode materials like LSC, LSCF and BSCF have both ionic and electronic conductivity (MIEC). Thus, oxygen which has been reduced by these cathodes can be conducted ionically to the electrolyte. Thus, ORR is not limited to TPB but takes place over the total surface of the cathode.

In addition to the cathode, the choice of electrolyte is also essential in IT-SOFC. In this respect, ScSZ as the electrolyte is particularly noteworthy as it displays a considerably high ionic conductivity at intermediate temperatures. In the present

study, we have selected ScSZ as an electrolyte. This restricts the choice of cathodes and thermal mismatch consideration yields LSM and LSF as suitable cathode material for ScSZ-based SOFCs (Kılıç et al. 2021).

As stated above, one of the effective strategies to enhance the overall performance of SOFCs is to lower the polarization resistance of the cathode layer. Meanwhile, various techniques were used to improve the kinetics of cathodic reactions at intermediate operating temperatures. One of these techniques was to choose perovskite composites with high hetero-structures to boost ORR (Sase et al. 2008).

The advantages of LSM as a cathode material are compatibility with zirconia-based electrolytes, sufficient catalytic activity, and acceptable electrical conductivity in the intermediate operating temperatures. Using LSM as a single material for cathode is not favored because of the sluggish electrochemical performance at the intermediate working temperatures. The best route is to produce a composite cathode. One of the oxides that can be used for this purpose is LSF, i.e LSM-LSF composite.

The goal of the present study was to develop LSM-LSF composite cathodes with a composition optimized for improved electrochemical performance. In order to reach this goal, thin composite films as the cathode were deposited on the ScSZ electrolytes in combinatorial geometry. The performance of these cathodes was tested on symmetrical cells via electrochemical impedance spectroscopy (EIS).

The thesis is made up of 4 chapters. Chapter 2 gives a literature review on cathode materials for IT-SOFCs. Chapter 3 gives experimental procedures used in the synthesis of multiphase cathodes as well as the procedures used for their electrochemical characterization. Chapter 4 reports results on LSM-LSF dual-phase cathodes which have been synthesized via sputter deposition. Finally, Chapter 5 gives general conclusions derived from the present study.

CHAPTER 2

LITERATURE REVIEW

In this section, we will first review electrolyte and anode materials for solid oxide fuel cells. Then cathode materials will be reviewed with an emphasis on IT-SOFCs.

2.1 Electrolytes

In the last decades, the field of searching for suitable materials as the electrolyte in IT-SOFCs is generally dominated by fluorite-type oxides with cations with FCC structure and anions in their tetrahedral sites. Oxygen ion vacancies which are essential for oxygen ion conduction, are produced when lower valence cations are inserted into the crystal structure. Fluorite-type electrolytes cover stabilized ZrO_2, doped CeO_2, and stabilized Bi_2O_3 (Bai et al. 2007).

The crystal structure of pure ZrO_2 up to 1170°C is monoclinic, which changes to tetragonal in the temperature range of 1170-2370°C and only above 2370°C it has the cubic structure (Terki et al. 2006). Due to the volume alteration during phase transformation, ZrO_2 can not maintain its stability during heating or cooling. The best strategy is to stabilize the cubic structure of pure ZrO_2 via a partial substitution of the Zr with trivalent or divalent cations. This not only stabilizes the cubic structure but also increases the oxygen ion conductivity by enhancing the oxygen vacancies.

There are many examples of stabilized zirconia, e.g., yttria-stabilized zirconia (YSZ), calcia-stabilized zirconia (CSZ), Scandia-stabilized Zirconia (ScSZ) or Manganese-stabilized zirconia (MSZ) (Li et al. 1994). Of these YSZ is the most popular electrolyte for conventional SOFC and has been used in many large-scale SOFC stacks with a power range of 1KW to 1MW (Han et al. 2006).

The best doping level in YSZ, as stated by Badwal (2001), was at 8% yttria. YSZ has many other outstanding advantages, like electronic insulation and compatibility with commonly used anode materials e.g. Ni-YSZ (Zakaria et al. 2019). The ionic conductivity of YSZ, while quite acceptable at elevated temperatures shows a drop at reduced temperatures typical of the operating temperature of IT-SOFCs. To compensate for this sluggish performance in lower operating temperatures, the best strategy is to make the electrolyte layer as thin as possible. Onbilgin et al. (2019) have compared different YSZ electrolyte fabrication techniques in terms of their effect on the performance of anode-supported SOFCs. They concluded that the tape casting is far better than both dip coating and screen-printing techniques. They further showed that the tape-cast electrolytes yielded the highest performance in all electrolyte sintering and cell operating temperatures. Their best performance was obtained with tape cast electrolytes sintered at 1400°C which yielded a peak performance of 0.924 W/cm^2 at 800°C, NiO-YSZ used as the anode, the cathode was a double layer oxide made up of LSM/YSZ (wt. % 50/50) and LSM.

CeO_2 is another important electrolyte material that has a cubic fluorite structure; like pure ZrO_2.The main problem with pure CeO_2 is its low oxygen ion conductivity. The strategy used in zirconia is also beneficial for ceria. Thus, the exchange of Ce^{4+} with trivalent and divalent cations like Gd^{3+}, Sm^{3+}, Y^{3+}, $La^{3+,}$ or Ca^{2+} is beneficial in improving its ionic conductivity. Hernandez et al. (2017) investigated the properties of deposited GDC-10 thin films as the electrolyte utilizing the reactive magnetron sputtering. In this study, they used tape-cast NiO-GDC as the anode layer. They successfully deposited dense, crack-free GDC electrolytes with 6μm thickness. In another study, Agarkova et al (2020) successfully deposited GDC electrolytes using the magnetron sputtering technique. In this study, bi-layered substrates were used as anode made up of NiO and $Sc_2O_{3,}$ the latter was co-stabilized with Y_2O_3 They have reported power density values of 1.8, 1.4, and 0.9 W/cm^2 for 800, 750 and 700ºC respectively.

Scandium-stabilized zirconia (ScSZ) is another attractive electrolyte material. ScSZ has the highest ionic conductivity at the intermediate operating temperatures

between all the ZrO_2-based electrolytes, Fig. 2.1. As an example, the first Japanese-made 1kW SOFC made use of ScSZ electrolyte which incorporated a 68-cell stack with a satisfactory performance at 800°C (Mizutani et al. 1995). The conductivity of several compositions in the scandia–zirconia system (Sc_2O_3 content between 7.0 and 11.0 mol%) was investigated as a function of temperature and time. The conductivity was degraded as a function of time, both at 850 and 1000°C for all electrolytes. This was attributed to the presence of a rhombohedral phase ($Sc_2Zr_7O_{17}$) in ScSZ (Badwal 2001). Tao et al. (2013) compared different dopant levels of scandia and found that 8mol% Sc_2O_3 Zirconia possesses the highest conductivity. Kubrin et al. (2017) studied the addition of ceria as a third constituent on the mechanical properties of tetragonal ScSZ. Their results suggest that cerium-free electrolytes should be preferred for the fabrication of the electrolyte-supported planar SOFCs.

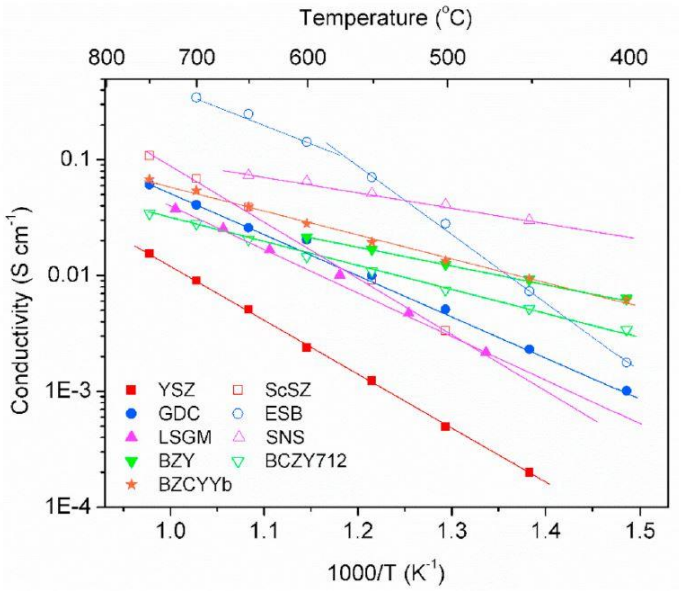

Figure 2.1. Ionic conductivity of various electrolytes used in SOFCs (Shi et al. 2020)

2.2 Anodes

After choosing the proper electrolyte material for SOFC, the next step is to choose the electrode materials which are compatible with the electrolyte layer. Cermets, i.e., sintered ceramic and metal compounds, are quite suitable as anode material. They have the advantage of having stable TPB zones, which is the main drawback of using single-phase metallic anodes as they sinter together at elevated temperatures. In order to make the anode more compatible mechanically and chemically, the oxide part is usually the same as the electrolyte material. The metallic constituents are usually either Ni or Cu. The metallic constituent makes the anode electronically conductive and the oxide part has the role of impeding the grain growth in the anode.

As stated above, YSZ is a common electrolyte material. Therefore, the anode chosen would be compatible with YSZ. Koide et al. (2000) investigated the Ni/YSZ cermet as the anode material for SOFC. They studied the performance of the anode in terms of power output, IR resistance, and polarization resistance as a function of the relative fraction of phases in Ni/YSZ. They found that the best performance was obtained with anodes with Ni/YSZ=40/60 composition. Ni/YSZ anode functions quite well when the fuel is hydrogen. However, they are quite vulnerable to sulfur or carbon poisoning when the input fuel is hydrocarbons, instead of hydrogen. Macek et al. (2006) prepared Ni-YSZ anodes using sol-gel and combustion synthesis and examined various dopants by exposing them to methane at high temperatures. They explained that the main reason for carbon deposition on the cermet was due to the thermal dissociation of methane and concluded that the carbon deposition may be minimized by controlling the anode composition and its microstructure.

Cu may also be used instead of nickel as a metallic constituent in the anodes. However, Cu has low catalytic activity in the case of using methane or other hydrocarbons as fuel. Gotsch et al. (2017) studied the carbon tolerance of Ni-Cu YSZ anodes using magnetron sputter deposition on Si wafers. They concluded that Cu/Ni=1, were not able to impede the carbon deposition completely and reported better performance when Cu/Ni >1. In another study by Costa-Nunes et al. (2004),

SOFCs with Cu-CeO_2-YSZ anodes were examined using H_2, CO, and syngas fuels. Their conclusion was that Cu-CeO_2-YSZ anodes had comparable performance using H_2 or CO as input fuels. However, Ni-YSZ anodes, also studied in this work, showed lower performance with CO compared to that with H_2. They investigated the effect of Co addition in Ni-YSZ to improve the performance and the results were more satisfactory with CO compared to H_2 at 973 K.

In the case of Gd doped ceria (GDC) electrolyte, many cermets with different compositions may be used as anodes; CuO-GDC, Ni Cu-GDC, NiO-GDC. De Marco et al. (2017) analyzed the performance of the cells with an anode consisting of 35 or 45 vol% CuO/GDC (Li-containing GDC electrolyte, LSCF/Li-GDC cathode) and concluded that increasing the copper content in the anode enhances the electronic conduction. They also report that with continued cell operation, Cu can migrate toward the anode/electrolyte interface. Iannucci et al. (2018) showed that the Cu/GDC cermet has high stability for IT-SOFCs with CH_4/CO_2 fuel. Acchar et al. (2017) used NiO-GDC produced by the aqueous tape casting method and sintered them at temperatures in the range of 1200 to 1400°C. They found that the tapes sintered at 1400°C had the highest density and acceptable porosities with mechanical strength up to 25 Mpa.

For ScSZ electrolytes, Ni-ScSZ anode is quite common as anode material due to its mechanical and chemical compatibility. Spirin et al. (2015) examined Ni-ScSZ in different compositions, and the lowest polarization resistance was achieved with 40 vol% Ni. In a study by Sumi et al. (2004), Ni-ScSZ was found to yield lower overpotentials than the Ni-YSZ due to the formation of amorphous graphite formed on the anode. In addition, a recent study done by Hagen et al. (2011) Ni-YSZ and Ni-ScSZ anodes showed improved performance in the case of sulphur containing fuel and that they are sulfur-tolerant. Matsui et al. (2012) have studied the anode stability in the presence of water vapor. They noted that Ni-YSZ cermets show an abrupt performance deterioration due to increased partial pressure of water vapor. They have compared the performances of Ni-YSZ, Ni-ScSZ, and Ni-SDC anodes in constant current operation. They found that there was no change in the performance of the cell with Ni–SDC anode,

whereas the ohmic resistances of the cells with Ni-YSZ and Ni-ScSZ anodes increased, implying sudden anode degradation.

2.3 Cathodes

Perovskites play a significant role as cathode materials for SOFC. Their chemical formula is ABO_3, and A stands for rare earth elements like Sr, La, Ca, Nd, Ba, or Pr, and B stands for Co, Ni, Fe, and Mn (Kaur et al. 2020). Generally, cathodes referred to above do not have sufficient performance in low temperatures. one of the commonly used perovskites is LSM. Its use in the pure form as a cathode for IT-SOFC is limited due to the high activation energy needed for oxygen dissociation and the sluggish conduction of oxygen ions. One strategy to improve this inactivity of LSM in terms of ionic transportation is to make mixtures of LSM with the used electrolyte material. In a study by Jeong et al. (2022) LSM-ScSZ composite cathodes were examined with different fractions. The best results were obtained with LSM: ScSZ=6:4 sintered at 1200°C and had the lowest total impedance value of 0.031 Ω cm^2 at 900°C.

(La, Sr)FeO_3 (LSF), $LaSrCoO_3$ (LSC), and $(La_{0.6}Sr_{0.4})_{0.99}Co_{0.2}Fe_{0.8}O$ (LSCF) are mixed ionic and electronic conductive (MIEC) cathodes. The MIEC materials not only provide the conduction of electrons for oxygen reduction reaction but also provides the ionic conduction required to ensure the transport of the reduced oxygen, thereby improving the overall electrochemical performance of the SOFC system (Burnwal et al. 2016).

LSC and in general Co-based cathodes have higher electronic and ionic conductivities in comparison to other materials. However, LSC chemically reacts with zirconia-based electrolytes (Keane et al. 2012), and also, due to their CTE compatibility issues, their use is not recommended with zirconia-based electrolytes. Solovyev et al. (2021) analyzed the performance of SOFC with multilayer LSC/GDC/LSC cathodes. The electrolyte was 8YSZ/GDC bilayer. Thin film cathodes were deposited with different combinations using the magnetron sputtering technique. The power density reached a value of 2430 $mW.cm^{-2}$ where each layer

was 50 nm thick. The corresponding polarization resistance cathode in this system was 0.17 and 0.3 Ω cm^2 at 800 and 700°C, respectively.

Another category of cathode materials is based on Fe as a B element. Their ionic conductivity is not as high as those of the LSC, but they are chemically stable with YSZ and other zirconia-based electrolytes, which makes them appropriate materials for the cathode in IT-SOFCs. The main issue with LSF is its lower conductivity which can be improved by doping. Thus, Simner et al. (2003) developed Sr-doped lanthanum ferrite cathodes for SOFC using a protective Sm-doped ceria (SDC) layer in between electrolyte and cathode so as to improve the performance of LSF in lower working temperatures.

The fourth category of common cathode materials is based on nickel. $La_2NiO_{4+\delta}$, $Nd_2NiO_{4+\delta}$, and $Pr_2NiO_{4+\delta}$ are layered perovskites. Han et al. (2011) studied the transport properties and electrochemical performance of cells with these layered oxides. They obtained the best electrochemical performance with the cell with $Pr_2NiO_{4+\delta}$ sintered at 1100°C where the maximum power densities were more than 0.2 $W.cm^{-2}$ at 800°C.

In recent years the so-called high entropy perovskite oxides were also used as cathodes. Yang et al. (2021) made use of a one-pot combustion method to synthesize a new type of as $La_{0.2}Pr_{0.2}Nd_{0.2}Sm_{0.2}Ba_{0.1}Sr_{0.1}Co_{0.2}Fe_{0.6}Ni_{0.1}Cu_{0.1}O_{3-\delta}$ (HEP). The final state of the proposed material was single-phase cubic perovskite, which was compatible with the YSZ and GDC electrolytes. Using YSZ electrolyte, they reported a polarization resistance of 0.3 $\Omega \cdot cm^2$ at 800°C. The output performance of the cell was 714.5 $mW.cm^{-2}$.

Shijie et al. (2022) synthesized A_2BO_4 type high entropy oxide namely $(La_{0.2}Pr_{0.2}Nd_{0.2}Sm_{0.2}Gd_{0.2})_2CuO_4$. The thermal expansion coefficient of this oxide was 12.19×10^{-6} K^{-1} in the range of 100–800 °C, which was compatible with GDC electrolyte. The measured area-specific resistance (ASR) was 0.52 $\Omega \cdot cm^2$ and the peak power density of this anode-supported system was 528 $mWcm^{-2}$ at 700°C.

The choice of the cathode in addition to fast ORR, should also take into account thermal mismatch with respect to the other components of the SOFC. ScSZ has a thermal expansion coefficient of 11.9×10^{-6}/°C (Tsipis et al. 2008). There are a number of matching electrodes with TEC close to this value. Of these LSM ($La_{0.5}Sr_{0.5}MnO_3$) and LSF ($La_{0.8}Sr_{0.2}FeO_3$), which have TEC of 11.5×10^{-6}/°C and 12.6×10^{-6}/°C respectively are particularly noteworthy (Tsipis et al. 2008). Of these LSF is a MIEC oxide as pointed out above. The reaction of the cathode with the electrolyte is also important. Wackerl et al. (2007) studied high-temperature reactions of LSM, LSCF, and SSM cathode with ScSZ electrolyte. After annealing the mixtures of cathode and electrolyte materials for 100 hours at 1200°C in air, it was found that the LSM-ScSZ mixture was affected little by this treatment, moreover LSM also showed a better adhesion with the ScSZ.

It may be pointed out that high entropy oxides used as cathodes in SOFC are usually single-phase oxides where many oxides are combined in a solid solution. The study of Sase et al. (2008) indicates that dual-phase cathode due to the presence of heterointerfaces results in accelerated ORR. This has been verified by Sari et al. (2018), who fabricated an LSC113-LSC214 dual-phase cathode via sputter deposition. They reported an ASR value of 0.15 ohm.cm^2 for LSC113:LSC214 = 0.45:0.55 at a temperature as low as 575°C. Moreover, the cathode produced was amorphous with a highly stable microstructure. This approach was further pursued by Kılıç et al. (2021) with a ternary system, namely LSM/LSF/ScSZ. A wide range of compositions was studied; the most favorite compositions were $LSM_{77}LSF_{11}ScSZ_{12}$ and $LSM_{72}LSF_{16}ScSZ_{12,}$ where an ASR value of 0.15 ohm.cm^2 was obtained at 805°C. However, the oxides at 805°C were crystalline. The most favorable compositions were close to the LSM-LSF binary, implying that binary oxides or compositions lean in ScSZ might yield a better cathode for IT-SOFCs.

CHAPTER 3

EXPERIMENTAL PROCEDURE

3.1 Synthesis of Active Materials

Active materials synthesized in the present work were LSM, LSF, and ScSZ. The precursors used were nitrates, namely; $La(NO_3)_3.6H_2O$ (Alfa Aesar, 99.99%), $Fe(NO_3)_3.9H_2O$ (Alfa Aesar, 99.99%), $Sr(NO_3)_2$ (Alfa Aesar, 99%), $Mn(NO_3)_2.H_2O$ (98%) and $ZrO(NO_3)_2.6H_2O$ (99%), $Sc(NO_3)_3.4H_2O$ (Nanografi, 99.9%).

The active materials were synthesized using the Pechini method (M.P. Pechini, 1967), Figure 3.1. The process involves; i) Nitrates, the amount of which are determined by aimed stoichiometry, put into a beaker and made a mixture by adding deionized water. After making the solution, citric acid of a controlled amount is added to the mixture. ii) The solution was mixed using a magnetic stirrer for 20 minutes at 80°C. iii) In the third step, ethylene glycol was added to the solution while it is being stirred. iv) Then the temperature was increased to 150°C, and heating continued until all solvents evaporated, resulting in dried gel-like material. v) The dried gel was then calcined at 850°C for 5 hours. Finally, after calcination, the resulting powders were ground with a mortar, yielding powders to be used for synthesis.

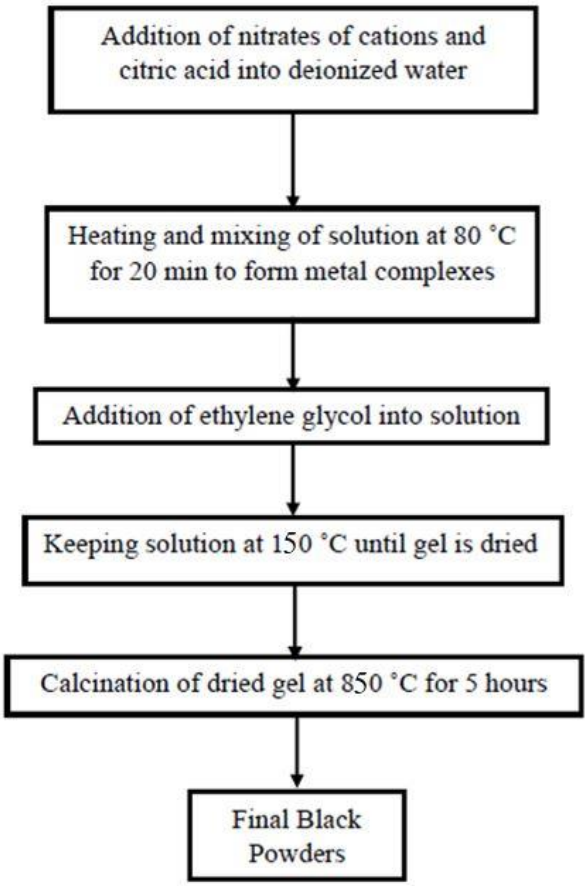

Figure 3.1. Flow chart of the Pechini process for synthesizing the active powders. (M.P. Pechini, 1967)

3.2 Preparation of Electrolyte Discs

For the production of ScSZ electrolyte substrate, the tape casting method is the most efficient one. Therefore, tape casting was chosen to fabricate the electrolyte layers. The electrolyte should be as thin as possible to decrease the ohmic resistance of the electrolyte.

For the fabrication of ScSZ layer, alcohol-based slurry systems were used in this work. The slurry was prepared in two steps. The first step involves mixing the active material, solvent, and dispersant. After mixing, ball milling was applied. The second step involves

the addition of a binder and plasticizer to the ball mill. The slurry was then cast onto mylar film. The film used for this purpose had a silicone coating for easy removal of the casting.

In order to determine the sintering regime, TGA measurement was taken. Then three different temperatures (1350°C, 1450°C, and 1550°C) were selected for the initial sintering experiments of which 1350°C was chosen as the sintering temperature for the layers.

3.3 Preparation of Sputter Targets for Cathode

Sputter targets of LSM and LSF were prepared from the synthesized powders. To do this, first, the powders were pressed by using deformable Teflon dies. Dies used had a 56 mm inner diameter with a 5 mm wall thickness and 5 mm in height. The compaction was carried out at pressures ranging from 64 MPa to 121 MPa. The compacts were then sintered at selected temperatures between 1300 to 1500°C. This has yielded sputter target discs which were slightly larger than 2 inches in diameter. The targets were ground to a diameter of 2 inches.

3.4 Sputter Deposition of Thin Film Cathodes

Thin film cathodes were deposited using a magnetron sputtering vacuum deposition system with a cubic chamber $500 \times 500 \times 500$ mm in dimensions, Figure 3.2. The experiments were carried out with the two sputter guns with target in tilted position where center-to-center distance was 125 mm. Sputter targets used were 2 inches in diameter.

Electrolyte substrates were in the form of 18 mm circular discs. They were placed in substrate holder, (Fig. 3.3) which was typically 110 mm above the center of the targets. Sensors close to the edges of substrate holder were used to monitor the thickness the film resulting from sputter deposition.

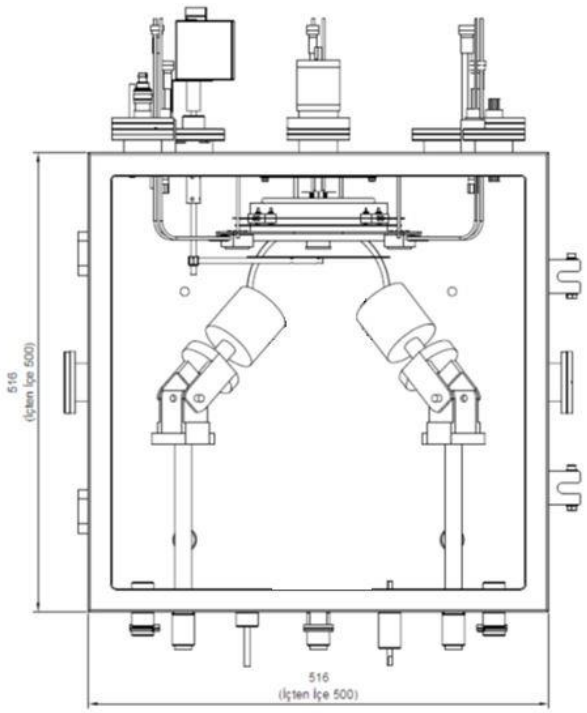

Figure 3.2. Sectional view of Sputter deposition chamber.

Figure 3.3. Sample holder used for sputter deposition of cathode materials.

(a) (b)

Figure 3.4. (a) Schematic representation of combinatorial deposition (b) View from the vacuum chamber with combinatorial deposition.

3.5 Materials and Electrochemical Characterization

Structural characterization is carried out using X-ray diffraction. For his purpose, the D/MAX-2200 Rigaku X-Ray diffractometer was used with a scanning rate of 2°/min using Cu-Kα radiation. Where necessary, X-ray data was refined using MAUD software (Lutterotti et al. 2000). Microstructural observations were carried out using FEI Nova Nano-SEM 430. Where necessary chemical analyses were determined using the EDS detector.

Electrochemical characterizations were carried out on symmetric cells. A schematic representation of the cell is given in Fig. 3.5 For this purpose, circular ScSZ electrolytes 18mm diameters and 100 μm thick were placed in the sample holder in a sputter deposition system, Fig. 3.2. Cathodes, typically 500 nm thick, were coated via co-sputtering of LSM and LSF targets. The discs were then turned over and the cathodes were also deposited on the backside of the cathodes. The cathodes as deposited on the electrolyte were 12 mm in diameter. Gold current collectors 150 nm in thickness, as shown in Fig 3.5. were coated over the cathode where the diameter was 10 mm.

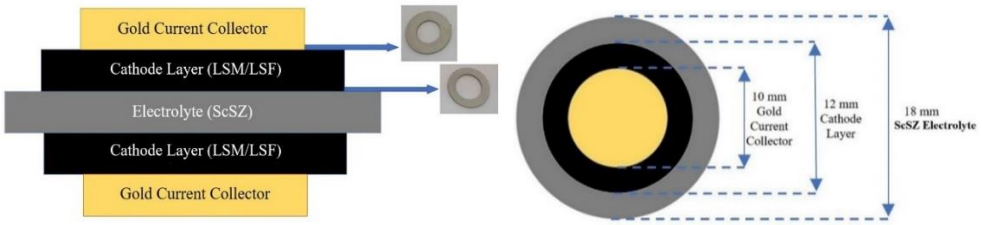

Figure 3.5. Schematic representation of symmetrical cells used for EIS measurements.

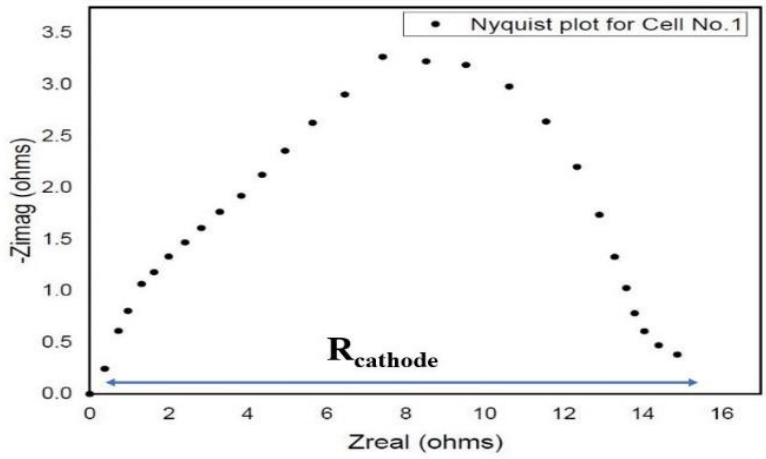

Figure 3.6. A typical example of EIS spectra. The example refers to co-sputtered symmetric cells LSM: LSF=0.7:0.93.at 700°C.

The symmetric cell, as described above, were installed to one end of an alumina tube. The cell was located at one end of the tube and sealed with the use of ceramic sealant. The whole assembly was placed inside a tubular furnace. EIS spectra were recorded on the symmetric cell using Gamry reference 3000 Potensiostat/Galvanostat. The contacts were made using gold wires attached to the gold coating using a silver paste. The spectra were recorded with 10mV perturbation voltage, the frequency in the range between 0.1Hz and 0.3Mhz.

From EIS spectra, $R_{cathode}$ is calculated from the Nyquist plots of EIS measurements, Figure 3.6. From $R_{cathode}$ area, specific resistance (ASR) values were determined using the:

$$ASR = \frac{R_{Cathode} \times [(\pi \times 0.6^2) - (\pi \times 0.5^2)]}{2} = \frac{R_{Cathode} \times 0.34}{2} \ (\Omega.cm^2)$$

Here D_e (0.6 cm) and D_i (0.5 cm) relate to the diameters of the cathode exposed to the atmosphere, i.e., not covered by gold contact.

CHAPTER 4

RESULTS and DISCUSSION

4.1 Synthesis of LSF and LSM Powder

Synthesis of LSF Powder: LSF with a $(La_{0.8}Sr_{0.2})FeO_{3-\delta}$ stoichiometry was synthesized using the Pechini method (M.P. Pechini, 1967). The precursors used were $La(NO_3)_3.6H_2O$, $Sr(NO_3)_2$ and $Fe(NO_3)_3.9H_2O$. Table 4.1. Citric acid and ethylene glycol used for sol-gel processing are also included in Table 4.2.

Table 4.1. Precursors used for $(La_{0.8}Sr_{0.2})FeO_{3-\delta}$ (LSF) synthesis.

$(La_{0.8}Sr_{0.2})FeO_{3-\delta}$ (M=232.5 gm)	Molar Mass (M)	Amount (gm)	Mole
$La(NO_3)_3.6H_2O$	433.10	1.84	0.0042
$Sr(NO_3)_2$	211.63	0.22	0.00105
$Fe(NO_3)_3.9H_2O$	404.00	2.121	0.00525

Table 4.2. The amounts of citric acid and ethylene glycol used for LSF sol-gel processing.

	Molar Mass (M)	Amount (gm)	Mole
Citric acid	192.12	50.95	0.2424
Ethylene glycol	62.07	60.00	0.9699

Dried gel was calcined at 800°C. The XRD pattern obtained from the resulting powder is given in Figure 4.1. The peak positions are consistent with LSF (JCPDS Card No. 00-035-1480). The pattern was Rietveld refined using a CIF file (Jennings et al. 2003) where the peaks fully fit standard LSF. The lattice constants are tabulated in Table 4.3. The calcined LSF powder was subjected to a detailed EDS analysis. EDS

analysis of LSF, calcined at 800◦C-5h, averaged for five different locations are given in Table 4.3.

Table 4.3 EDS analysis (average) for LSF powder calcined at 800°C for 5 hours.

LSF	Measured at%
La	41.0
Sr	10.4
Fe	48.6

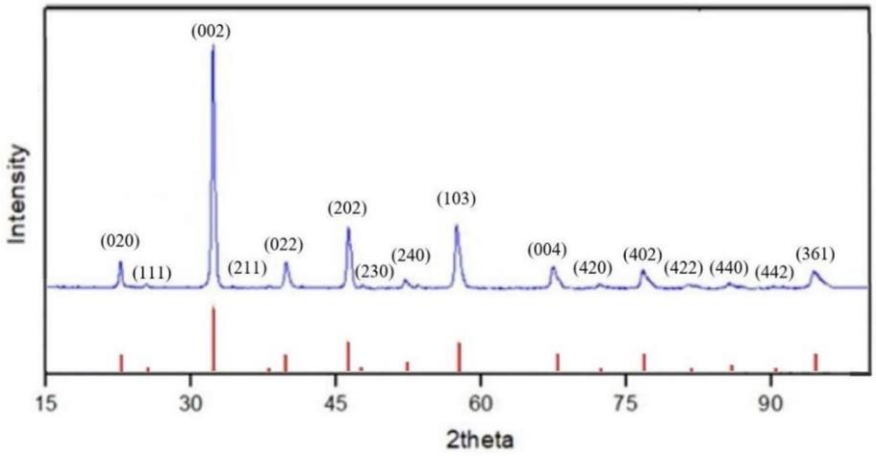

Figure 4.1. XRD pattern of LSF calcined at 800°C for 5 hours.

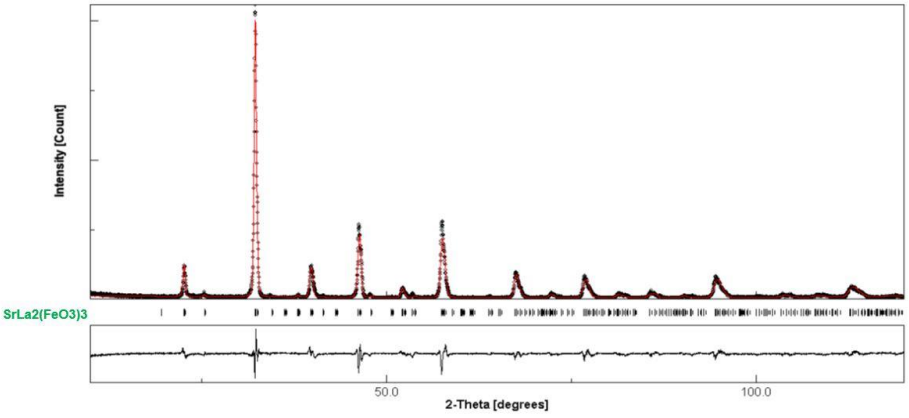

Figure 4.2. Rietveld refined XRD pattern of LSF calcined at 800°C.

Table 4.4 Lattice constants of LSF, LSM, and ScSZ powders synthesized by the Pechini method calcined at 800°C for 5 hours.

	Lattice Constants (Å)		
	a	b	c
LSM	5.445	5.445	7.759
LSF	5.536	7.836	5.550
ScSZ	5.098		

Synthesis of LSM Powder: LSM with a $(La_{0.5}Sr_{0.5})MnO_{3-\delta}$ stoichiometry was synthesized using the Pechini method. (M.P. Pechini, 1967) The precursors used were $La(NO_3)_3.6H_2O$, $Sr(NO_3)_2$ and $Mn(NO_3)_2.6H_2O$. Table 4.5. Citric acid and ethylene glycol used for sol-gel processing are also included in Table 4.6.

Table 4.5. Composition of the precursors used for $(La_{0.5}Sr_{0.5})MnO_{3-\delta}$ (LSM) synthesis.

$(La_{0.5}Sr_{0.5})MnO_{3-\delta}$ (M=216.2 gm)	Molar Mass (M)	Amount (gm)	Mole
$La(NO_3)_3.6H_2O$	433.10	3.77	0.0087
$Sr(NO_3)_2$	211.63	1.84	0.0087
$Mn(NO_3)_2.6H_2O$	286.95	5.00	0.0174

Table 4.6. The amount of citric acid and ethylene glycol used for LSM sol-gel processing.

	Molar Mass (M)	Amount (gm)	Mole
Citric acid	192.12	20.08	0.1045
Ethylene glycol	62.07	25.95	0.4181

Dried gel was calcined at 800°C. The XRD pattern obtained from the resulting powder is given in Figure 4.3. The peak positions are consistent with JCPDC card

No. 01-077-4313. The pattern was Rietveld refined using a CIF file (Kubota et al., 2000) where the peaks fully fit LSM. The calcined LSM powder was subjected to a detailed EDS analysis of the elemental distribution. EDS analysis of LSM, calcined at 800◦C-5h, averaged for five different locations are given in Table 4.7.

Table 4.7 EDS Analysis (average) for LSM powder calcined at 800°C for 5 hours.

LSM	Measured at%
La	26.5
Sr	26.5
Mn	47.0

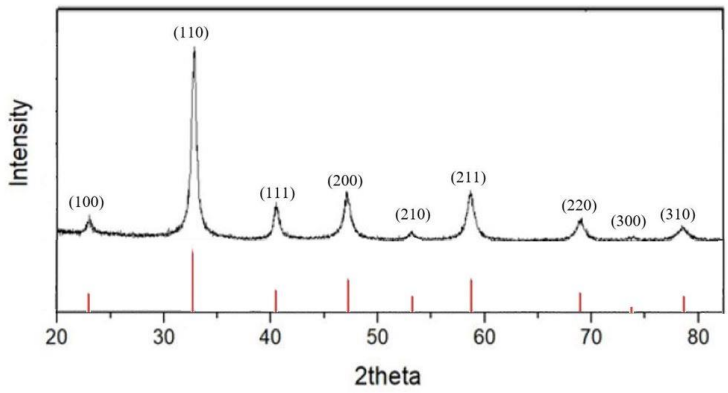

Figure 4.3. XRD pattern of LSM calcined at 800°C for 5 hours.

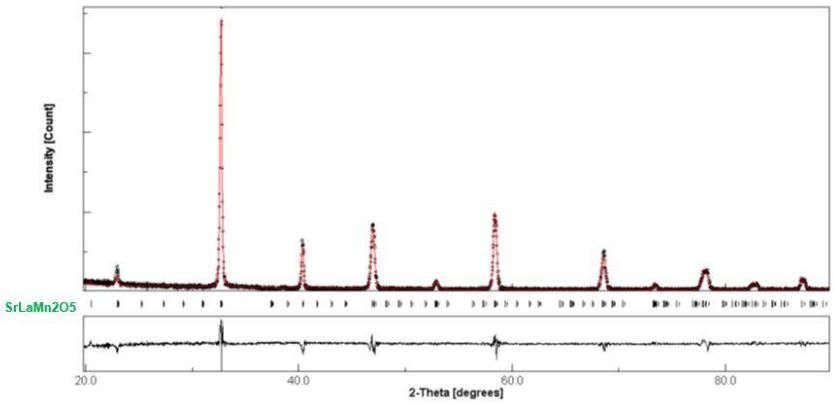

Figure 4.4. Rietveld refined XRD pattern of LSM calcined at 800°C.

4.2 Synthesis of ScSZ Powder

ScSZ with a $Sc_{0.15}Zr_{0.85}O_{2-\delta}$ stoichiometry was synthesized using the Pechini method (M.P. Pechini, 1967). The precursors used were $Sc(NO_3)_3.4H_2O$, $Zr(NO_3)_2.6H_2O$. Table 4.8. Citric acid and ethylene glycol used for sol-gel processing are also included in Table 4.9.

Table 4.8. Composition of the precursors used for $Sc_{0.15}Zr_{0.85}O_{2-\delta}$ (ScSZ) synthesis.

($Sc_{0.15}Zr_{0.85}O_{2-\delta}$ M=112.5 gm)	Molar Mass (M)	Amount (gm)	Mole
$Sc(NO_3)_3.4H_2O$	302.97	1.00	0.0030
$Zr(NO_3)_2.6H_2O$	339.23	6.34	0.0180

Table 4.9. The amount of citric acid and ethylene glycol amount used for ScSZ sol-gel processing.

	Molar Mass (M)	Amount (gm)	Mole
Citric acid	192.12	12.68	0.0660
Ethylene glycol	62.07	16.38	0.2640

Dried gel was calcined at 850°C. The XRD pattern obtained from the resulting powder is given in Figure 4.5. The peak positions are consistent with standard JCPDS 01-089-5480. The pattern was Rietveld refined using a CIF file (Barker et al., 1973) where the peaks fully fit standard ScSZ. The calcined ScSZ powder was subjected to a detailed EDS analysis of the elemental distribution. EDS analysis of ScSZ, calcined at 850◦C-5h, averaged for five different locations are given in Table 4.10.

Table 4.10 EDS analysis (average) for ScSZ powder calcined at 850°C for 5 hours.

ScSZ	Measured at%
Sc	15.6
Zr	84.4

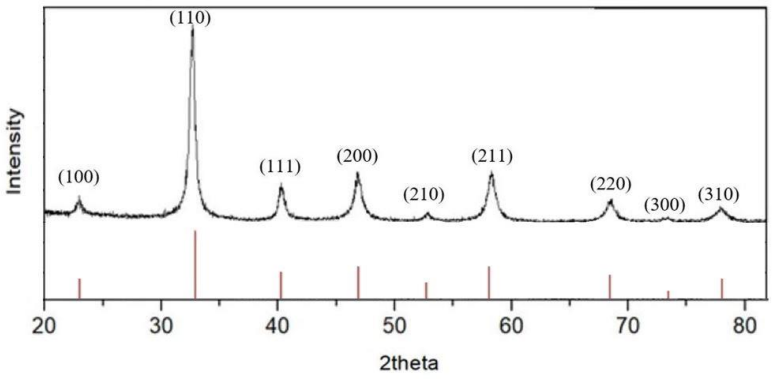

Figure 4.5. XRD pattern of ScSZ calcined at 850°C for 5h.

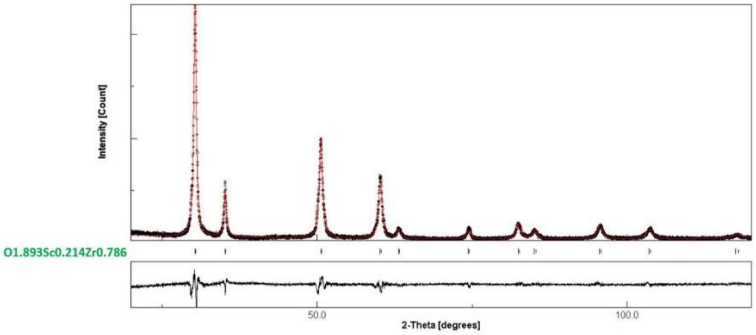

Figure 4.6. Rietveld refined XRD pattern of ScSZ calcined at 850°C.

4.3 Preparation of Electrolyte Discs

Electrolyte discs were prepared by a tape casting method (Wang et al. 2008). This involves the preparation of a slurry and the casting of electrolyte discs. Ingredients used for the preparation of electrolyte slurry are given in Table 4.11. The slurry was prepared in two steps. The first step involves mixing the active material, solvent, and dispersants. After mixing, ball milling was applied for 2 hours at 100 rpm with 10mm zirconia balls. The second step involves the addition of a binder and plasticizer into the ball milling jar. The ball milling was then continued for another 2 hours. The blade gap was adjusted to 350 μm, and the slurry was cast at a speed of 7mm/sec. The casting was carried out onto a mylar film. The film used for this purpose had a silicone coating for easy removal of the slip. The slip was dried in open atmosphere for 2 hours and 20 mm diameter discs were punched from the electrolyte.

Table 4.11. Amount of ingredients used in preparing electrolyte slurry.

Active Material	Solvent		Dispersant	Binder	Plasticizer
ScSZ	MEK	EtOH	Triethanolamine	Polyvinyl Butyral	Polyethylene glycol
4.24 gm	2.60 ml	2.60 ml	0.17 gm	0.44 gm	0.44 gm

The electrolyte discs were then sintered at elevated temperatures. In order to determine the sintering regime, TGA measurement was taken up to 800°C. (This measurement was taken from anode-elctrolyte bilayer but considered to be valid also for the electrolyte on its own). As seen in Figure 4.7. a decrease in mass starts from 50°C and accelerates after 200°C. The mass loss becomes less after 250°C, and it is almost complete by 475°C. Based on this measurement, discs were heated at a rate of 0.5°C/min up to 250°C where it was kept for an hour. Then it was continued heating with the same rate (0.5°C/min) up to 700°C. The heating rate was then increased to 1.5°C/min and continued up to 1350°C and maintained there for 2.5 hours. Discs were then cooled to room temperature at a rate of 1.5°C/min.

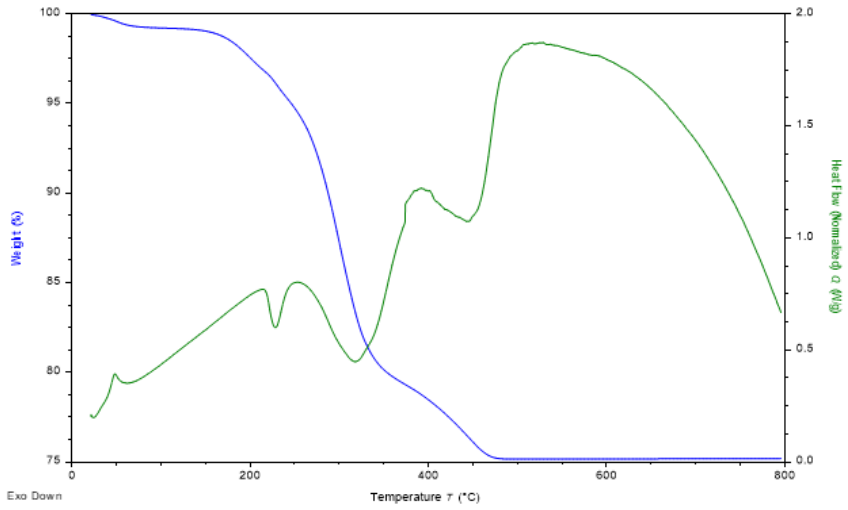

Figure 4.7. Thermal gravimetric analysis (TGA) of anode-electrolyte bilayer.

4.4 Fabrication of Sputter Targets for Cathodes

LSM Target: As reported above, powders were compacted using a deformable Teflon die. Following preliminary experiments, LSM powders were compacted with 140 MPa using a Teflon die with a diameter of 56 mm, 5mm height, and a wall thickness of 5mm. The compact was then sintered at 1500°C for 3 hours. This led to a shrinkage of approximately 10%, where the diameter was about 52 mm. The target was ground carefully so as to reduce the diameter to a value between 50 and 51mm. The sputter target produced is given in Figure 4.8. (a).

LSF Target: Based on preliminary experiments, LSF powders were compacted with a pressure of 140 MPa. The deformable die had dimensions of 65 mm diameter, 5mm height, and a wall thickness of 5mm. Sintering was carried out at 1500°C for 5 hours. The radial shrinkage of the powders was 27%. The resulting disc was grounded carefully so that the diameter of the disc was between 50-51 mm, Figure 4.8. (b).

(a) (b)

Figure 4.8. Sputter targets (a) LSM, (b) LSF

4.5 Combinatorial Deposition of Cathodes

LSM and LSF sputter targets were placed in the sputter guns, which were 125 mm apart, as explained in the experimental section. The sample holder was 110 mm above the center of the sputter targets. Parameters used in sputter deposition are reported in Table 4.12. Guns were aligned using glass substrates by measuring the thickness of the deposited layer. Substrates used were glass. The reason for choosing glass substrate was due to the fact that it can be easily broken, and the cross-section

can be examined in SEM, allowing the determination of the film thickness. Power loading on each sputtering target was adjusted so that the film thickness at both ends of the sample holder (i.e., substrate no. 1 and substrate no. 6) had similar thickness values.

Table 4.12 Parameters used in sputter deposition of cathodes on the glass substrate.

Initial Pressure (Torr)	**Sputtering Pressure (mTorr)**	**Argon Flow Rate (sccm)**	**Oxygen Flow Rate (sccm)**
1.1×10^{-6}	5	20	5

Target	**Duration (min)**	**Sensors (kÅ)**	**Rate (Å/s)**	**RF Power (Watt)**	**Measured SEM (nm)**
LSM	180	0.148	0.085	110	92
LSF	180	0.152	0.088	11	96

Table 4.13 Parameters used in sputter deposition of cathodes on Aluminum and ScSZ Electrolyte discs.

Initial Pressure (Torr)	**Sputtering Pressure (mTorr)**	**Argon Flow Rate (sccm)**	**Oxygen Flow Rate (sccm)**
8.15×10^{-7}	5	20	5

Target	**Duration (h)**	**Read by Sensors (kÅ)**	**RF Power (Watt)**	**Read by SEM (nm)**	**Rate (Å/s)**
LSM	16	0.789	110	460	0.079
LSF	16	0.815	11	500	0.087

The power loading used was 110 watts for LSM and 11 watts for LSF, Table 4.12. This has yielded a film thickness of approximately 100 nm for a co-sputtering duration of 3 hours. Guns were further aligned so that the film thickness in the middle (substrate No 4) was within 10% of the average. This alignment involved changing the tilt of the gun while maintaining the same distance between the center of the sputter target and the substrate plane.

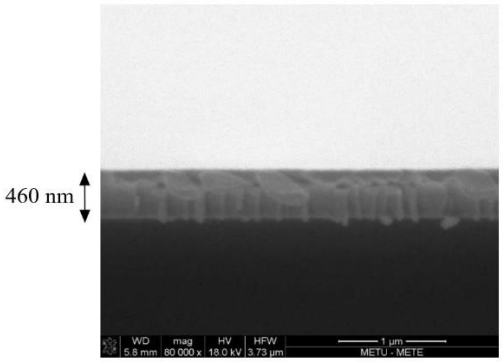

Figure 4.9. SEM image of cathode deposited on a glass substrate for 16 hours (Substrate in position 3)

Two sets of deposition were carried out, each with a duration of 16 hours. One set was deposited on glass substrates. A typical example of the deposited film on a glass substrate is given in Figure 4.9. Following this experiment, a second experiment was carried out on aluminum substrate in exactly the same conditions.

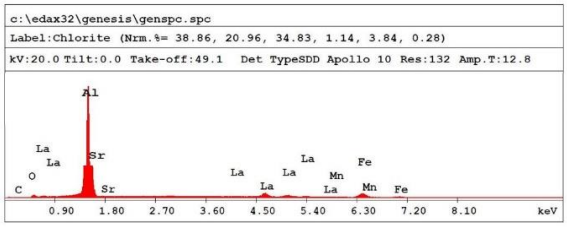

EDAX ZAF Quantification (Standardless)
Element Normalized
SEC Table : Default

Element	Wt %	At %	Z	A	F
SrL	3.42	3.26	0.9864	0.5596	1.0020
LaL	53.47	32.17	0.9177	1.0200	1.0303
MnK	2.10	3.20	1.0725	0.8972	1.0000
FeK	41.01	61.37	1.0964	0.9049	1.0000
Total	100.00	100.00			

Figure 4.10. EDS spectra and elemental composition of sample No.1 deposited on aluminum substrate.

Deposition on aluminum substrates was used for EDS analysis of co-sputtered cathodes. A typical example of EDS analysis is given in Figure 4.10, which refers to substrate No. 1. Chemical analysis of co-sputtered cathodes is given in Table 4.14.

Table 4.14. Composition of co-sputtered cathode thin films measured by EDS analysis.

Sample	**Atomic %**				
No.	**La**	**Sr**	**Fe**	**Mn**	**Mn/Fe**
1	31.59	3.13	60.69	4.58	0.07
2	32.48	6.29	51.78	9.43	0.18
3	29.04	12.17	42.38	16.4	0.38
4	28.48	13.92	33.47	24.12	0.72
5	27.79	14.98	25.75	31.46	1.221
6	29.62	8.89	23.53	37.94	1.612

Table 4.15. Calculated composition (molar) of co-sputtered cathode thin films.

Sample No.	**Mn/Fe**	**Mole fraction LSM**	**Mole fraction LSF**	**At% (Expected values)**			
				La	**Sr**	**Fe**	**Mn**
1	0.07	0.07	0.93	38.93	11.06	46.45	3.55
2	0.18	0.15	0.85	37.69	12.31	42.30	7.70
3	0.38	0.28	0.72	35.81	14.18	36.05	13.95
4	0.72	0.42	0.58	33.71	16.28	29.05	20.95
5	1.22	0.55	0.45	31.75	18.25	22.50	27.50
6	1.61	0.62	0.38	30.73	19.27	19.10	30.90

Two elements in Table 4.13 are important in determining the molar makeup of the cathodes. These are Mn and Fe, which represent LSM and LSF, respectively. The mole fraction of LSM and LSF calculated from the atomic fraction of Mn and Fe are tabulated in Table 4.15. It is seen that the composition in position 1, LSM: LSF= 0.07:0.93, changes systematically and reached LSM: LSF = 0.62:0.38 in position 6.

Also included in Table 4.14 are elemental compositions (at%) of the cathodes. Ideally, these values should match those reported in Table 4.15. The differences are quite significant, which probably arise from uncertainties from EDS measurement and due to differences in the stoichiometry of LSM and LSF.

4.6 Electrochemical Characterization via Symmetrical Cell

In order to monitor the electrochemical performance of fabricated thin film cathodes, symmetrical cells were produced using ScSZ electrolyte discs. ScSZ electrolyte discs 18mm in diameter were placed in the sample holder from position no. 1 to position no 6. Stainless steel rings (outside diameter: 18 mm, inside diameter: 12 mm) were placed over the disc so as to prevent the short circuit effect of cathodes.

Co-sputtering was carried out in exactly the same condition as in Table 4.13 for a total duration of 16 hours. Having finished the coatings, the electrolytes were turned upside down, and the experiment was repeated in the same condition and for the same duration. In this experiment, both sides of the electrolytes were coated with cathodes.

After finishing the cathode fabrication, symmetric cells were placed in a circular sample holder, Figure. 4.11. Stainless steel ring outside diameter of 18 mm inside diameter: of 10 mm was placed over the symmetric cell. While the sample holder was rotating (8rpm), the cells were coated with gold to a thickness of 150 nm.

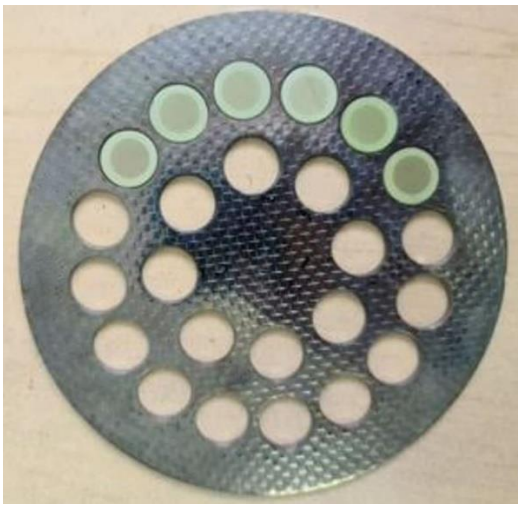

Figure 4.11. Sample holder used for gold coating of symmetric cells

The symmetric cell, as described above, was installed on one end of an alumina tube 25 mm in inner and 36 mm in outer diameter. The cell was located at one end of the tube and sealed with the use of ceramic sealant (AREMCO). The whole assembly was placed inside a tubular furnace, as shown in Figure 4.12. The symmetric cell at the end of the tube was located at the very center of the furnace, and measurements were carried out.

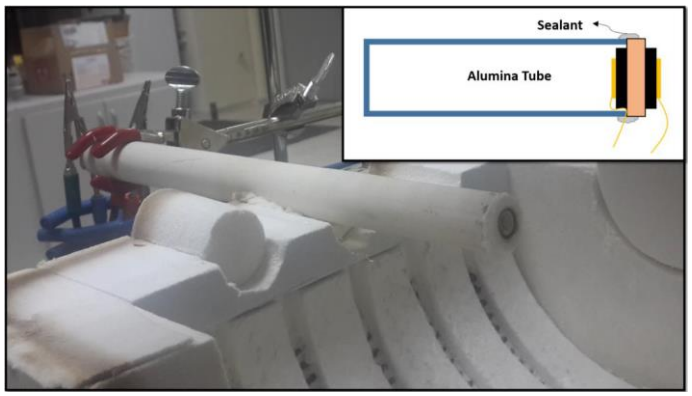

Figure 4.12. Assembly of the symmetric cell for EIS measurements in a tubular furnace; the inset indicates the schematic representation of the assembly.

Figure 4.13. Set-up to for carrying out EIS measurement on symmetric cells.

EIS spectra were measured on symmetric cells from 600 to 800°C with intervals of 50°C.

Table 4.16. ASR values as a function of temperature in LSM-LSF composite cathodes.

Composition\Temperature	**600°C**	**650°C**	**700°C**	**750°C**	**800°C**
LSM_7LSF_{93}	36.8	7.41	2	0.62	0.3
$LSM_{15}LSF_{85}$	120	19	3	1	0.65
$LSM_{28}LSF_{72}$	4.5	2.1	0.9	0.3	0.25
$LSM_{42}LSF_{58}$	1.95	1	0.7	0.2	0.12
$LSM_{55}LSF_{45}$	2.2	1.5	0.9	0.25	0.16
$LSM_{62}LSF_{38}$	50	6.5	2.5	0.7	0.3

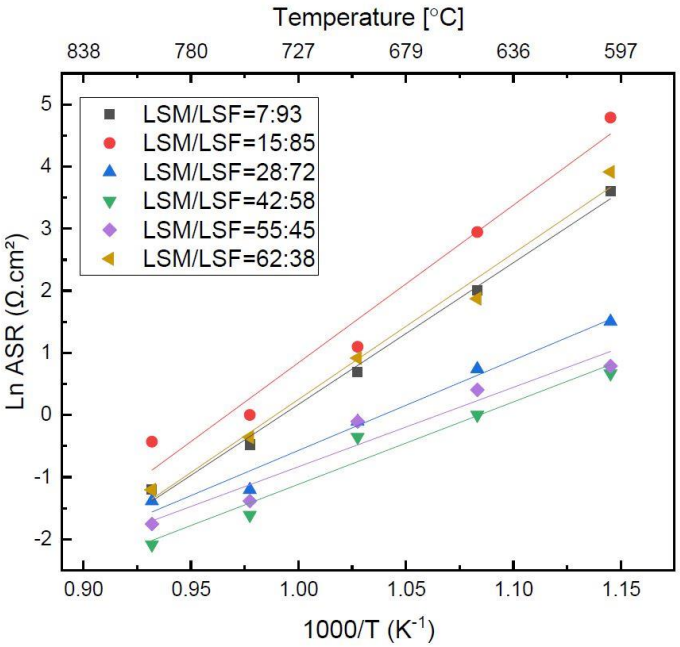

(a)

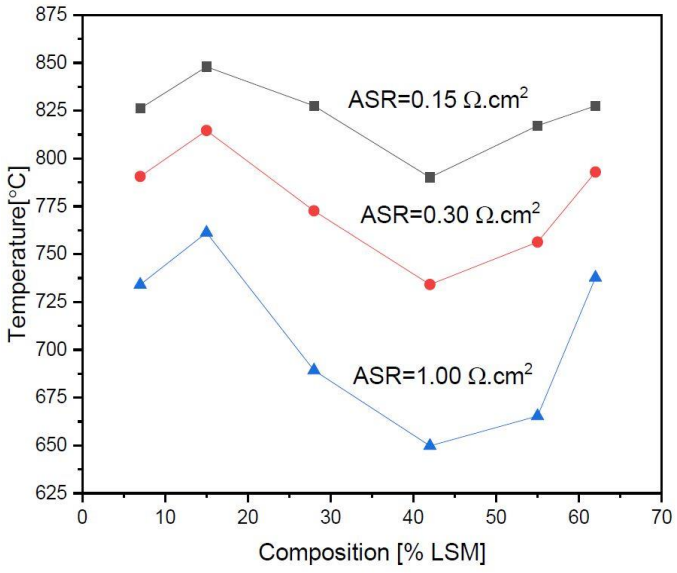

(b)

Figure 4.14. a) ln (ASR) versus 1000/T for cathodes with composition ranging from LSM: LSF=7:93 to LSM: LSF=62:38, b) Temperature predicted from (a) for the area specific resistance values of 0.15 Ω.cm^2, 0.30 Ω.cm^2 and 1.0 Ω.cm^2 as a function of compositions.

ASR values calculated for the composite cathodes are tabulated in Table 4.16. It is seen that with increasing temperature, ASR values show a pronounced decrease. It should be noted that the lowest area-specific resistance value was obtained in **$LSM_{42}LSF_{58}$** where ASR= 0.12 ohm.cm^2 at 800°C.

Ln (ASR) versus 1000/T plot was obtained from Table 4.16 and plotted in Figure 4.16 (a). Here horizontal lines were drawn at ASR= 0.15, 0.30 1.0 ohm.cm^2. The corresponding temperatures are plotted as a function of composition in Figure 4.16. (b). Here curves verify that ASR values are lowest where the composite comprises a comparable fraction of the constituent phases. Since 0.15 ohm.cm^2 is the benchmark for useful cathodes, Figure 4.16 imply that $LSM_{42}LSF_{58}$ cathode yields the lowest working temperature of 780°C.

Thus, the current work shows that composite cathodes based on LSM and LSF would yield cathodes where that can be used at temperatures close to 800°C, and that of these $LSM_{42}LSF_{58}$ yield the lowest ASR values with operating temperature as low as 780°C.

CHAPTER 5

CONCLUSIONS

In this thesis, a study was carried out on LSM-LSF composite cathodes for IT-solid oxide fuel cells. The study follows previous work carried out on LSM/LSF/ScSZ ternary composite cathodes and LSC113-LSC214 dual-phase cathodes, both developed for IT-SOFCs.

The study involved the synthesis of active material, namely $(La_{0.5}Sr_{0.5})MnO_{3-\delta}$ (LSM), $(La_{0.8}Sr_{0.2})FeO_{3-\delta}$ (LSF), and $Sc_{0.15}Zr_{0.85}O_{2-\delta}$ (ScSZ) via Pechini method. Symmetric cells were fabricated, and cathodes were characterized electrochemically via EIS measurements. For this purpose, ScSZ electrolyte discs were produced by the tape-casting method. The discs were used as the substrates on which cathodes of the same composition were deposited via sputter deposition on both sides of the electrolyte using sputter targets produced from the synthesized powders.

LSM/LSF composite cathodes with different compositions were obtained and were electrochemically characterized for temperatures ranging from 600 to 800°C with 50°C intervals. Composite cathodes with composition ranging from LSM: LSF=7:93 to LSM: LSF=62:38 were studied, yielding area-specific values which were, in general, less than ASR=0.3ohm.cm^2. The lowest temperature for which the benchmark value of ASR= 0.15 ohm.cm^2 was obtained was $LSM_{42}LSF_{58}$. This implies that this cathode can be used at temperatures as low as 780°C.

REFERENCES

A. Hagen, J.F.B. Rasmussen, K. Thydén, Durability of solid oxide fuel cells using sulfur containing fuels, in: J. Power Sources, 2011. https://doi.org/10.1016/j.jpowsour.2011.02.053.

Acchar, W., Cruz, L. B., & Paes Junior, H. R. (2018). Study of NiO-GDC material produced by aqueous tape casting. *Matéria (Rio De Janeiro)*, *22*(suppl 1). https://doi.org/10.1590/s1517-707620170005.0278

Agarkova, E. A., Agarkov, D. A., Burmistrov, I. N., Zadorozhnaya, O. Y., Yalovenko, D. V., Nepochatov, Y. K., & Bredikhin, S. I. (2020). Three-Layered Membranes for Planar Solid Oxide Fuel Cells of the Electrolyte-Supported Design: Characteristics and Applications. *Russian Journal of Electrochemistry*, *56*(2), 132–138. https://doi.org/10.1134/s1023193520020020

Badwal, S. (2001). Stability of solid oxide fuel cell components. *Solid State Ionics*, *143*(1), 39–46. https://doi.org/10.1016/s0167-2738(01)00831-1

Bai, B., McPhee, W. A., Smirnova, A. L., & Sammes, N. M. (2007). A Comparison and Characterization of CeO2-doped and Bi2O3-doped Scandia Stabilized Zirconia as IT-SOFC Electrolytes. *ECS Transactions*, *7*(1), 2213–2221. https://doi.org/10.1149/1.2729337

Barker, W., Bailey, F., & Garrett, W. (1973). A high-temperature neutron diffraction study of pure and scandia-stabilized zirconia. *Journal of Solid State Chemistry*, *7*(4), 448–453. https://doi.org/10.1016/0022-4596(73)90173-4

Bi, W., Gray, G. E., & Fuller, T. F. (2007). PEM Fuel Cell Pt/C Dissolution and Deposition in Nafion Electrolyte. *Electrochemical and Solid-State Letters*, *10*(5), B101. https://doi.org/10.1149/1.2712796

Burnwal, S. K., Bharadwaj, S., & Kistaiah, P. (2016). Review on MIEC Cathode Materials for Solid Oxide Fuel Cells. *Journal of Molecular and Engineering Materials*, *04*(02), 1630001. https://doi.org/10.1142/s2251237316300011

Chen, G., Guan, G., Kasai, Y., You, H. X., & Abudula, A. (2011). Performance of cathode-supported SOFC with Ni0.5Cu0.5–CGO anode operated in humidified hydrogen and in low-concentration dry methane. *Journal of Solid State Electrochemistry*, *16*(6), 2071–2077. https://doi.org/10.1007/s10008-011-1615-1

Chen, K., Lü, Z., Ai, N., Chen, X., Hu, J., Huang, X., & Su, W. (2007). Effect of SDC-impregnated LSM cathodes on the performance of anode-supported YSZ films for SOFCs. *Journal of Power Sources*, *167*(1), 84–89. https://doi.org/10.1016/j.jpowsour.2007.01.088

Chen, K., Lü, Z., Chen, X., Ai, N., Huang, X., Du, X., & Su, W. (2007). Development of LSM-based cathodes for solid oxide fuel cells based on YSZ films. *Journal of Power Sources*, *172*(2), 742–748. https://doi.org/10.1016/j.jpowsour.2007.05.035

Costa-Nunes, O., Gorte, R. J., & Vohs, J. M. (2005). Comparison of the performance of Cu–CeO2–YSZ and Ni–YSZ composite SOFC anodes with H2, CO, and syngas. *Journal of Power Sources*, *141*(2), 241–249. https://doi.org/10.1016/j.jpowsour.2004.09.022

De Marco, V., Iannaci, A., Rashid, S., & Sglavo, V. M. (2017). Effect of anode thickness and Cu content on consolidation and performance of planar copper-based anode-supported SOFC. *International Journal of Hydrogen Energy*, *42*(17), 12543–12550. https://doi.org/10.1016/j.ijhydene.2017.03.221

Götsch, T., Schachinger, T., Stöger-Pollach, M., Kaindl, R., & Penner, S. (2017). Carbon tolerance of Ni–Cu and Ni–Cu/YSZ sub-µm sized SOFC thin film model systems. *Applied Surface Science*, *402*, 1–11. https://doi.org/10.1016/j.apsusc.2017.01.076

Guangul, F. M., & Chala, G. T. (2020). A Comparative Study between the Seven Types of Fuel Cells. *Applied Science and Engineering Progress*, *13*(3). https://doi.org/10.14416/j.asep.2020.04.007

HAN, J., ZHENG, K., & ŚWIERCZEK, K. (2011). NICKEL-BASED LAYERED PEROVSKITE CATHODE MATERIALS FOR APPLICATION IN INTERMEDIATE-TEMPERATURE SOLID OXIDE FUEL CELLS. *Functional Materials Letters*, *04*(02), 151–155. https://doi.org/10.1142/s1793604711001853

H. Sumi, K. Ukai, Y. Mizutani, H. Mori, C.J. Wen, H. Takahashi, O. Yamamoto, Performance of nickel-scandia-stabilized zirconia cermet anodes for SOFCs in 3% H2O-CH4, Solid State Ionics. (2004). https://doi.org/10.1016/j.ssi.2004.06.016.

Han, M., Tang, X., Yin, H., & Peng, S. (2007). Fabrication, microstructure and properties of a YSZ electrolyte for SOFCs. *Journal of Power Sources*, *165*(2), 757–763. https://doi.org/10.1016/j.jpowsour.2006.11.054

He, S., Li, R., Ge, L., Chen, H., & Guo, L. (2013). Preparation and characterization of Cu–SDC anodes for low-temperature solid oxide fuel cell. *Journal of*

Alloys and Compounds, *576*, 242–246. https://doi.org/10.1016/j.jallcom.2013.04.143

Hernandez Londono, C., Combemale, L., Gao, F., Billard, A., & Briois, P. (2017). Properties of Gadolinium-doped Ceria (GDC) Films Deposited by Reactive Magnetron Sputtering Processes. *ECS Transactions*, *78*(1), 1189–1193. https://doi.org/10.1149/07801.1189ecst

Hussain, S., & Yangping, L. (2020). Review of solid oxide fuel cell materials: cathode, anode, and electrolyte. *Energy Transitions*, *4*(2), 113–126. https://doi.org/10.1007/s41825-020-00029-8

Jeong, H., Sharma, B., Jo, S., Kim, Y. H., & Myung, J. H. (2022). Electrochemical characteristics of La0.8Sr0.2MnO3 (LSM)–scandia-stabilized zirconia (ScSZ) composite cathode. *Journal of the Korean Ceramic Society*, *59*(4), 473–479. https://doi.org/10.1007/s43207-022-00200-5

Jennings, A., Skinner, S., & Helgason, Ö. (2003). Structural properties of La Sr2−FeO4± at high temperature and under reducing conditions. *Journal of Solid State Chemistry*, *175*(2), 207–217. https://doi.org/10.1016/s0022-4596(03)00248-2

Kaur, P., & Singh, K. (2020). Review of perovskite-structure related cathode materials for solid oxide fuel cells. *Ceramics International*, *46*(5), 5521–5535. https://doi.org/10.1016/j.ceramint.2019.11.066

Keane, M., Mahapatra, M. K., Verma, A., & Singh, P. (2012). LSM–YSZ interactions and anode delamination in solid oxide electrolysis cells. *International Journal of Hydrogen Energy*, *37*(22), 16776–16785. https://doi.org/10.1016/j.ijhydene.2012.08.104

Koide, H. (2000). Properties of Ni/YSZ cermet as anode for SOFC. *Solid State Ionics*, *132*(3–4), 253–260. https://doi.org/10.1016/s0167-2738(00)00652-4

Kubota, M., Fujioka, H., Hirota, K., Ohoyama, K., Moritomo, Y., Yoshizawa, H., & Endoh, Y. (2000). Relation between Crystal and Magnetic Structures of Layered Manganite $La_{2-2x}Sr_{1+2x}Mn_2O_7$(**0.30**≤x≤***0.50***). *Journal of the Physical Society of Japan*, *69*(6), 1606–1609. https://doi.org/10.1143/jpsj.69.1606

Kubrin, R., Blugan, G., & Kuebler, J. (2017). Influence of cerium doping on mechanical properties of tetragonal scandium-stabilized zirconia. *Journal of the European Ceramic Society*, *37*(4), 1651–1656. https://doi.org/10.1016/j.jeurceramsoc.2016.11.038

Li, P., Chen, I. W., & Penner-Hahn, J. E. (1994). Effect of Dopants on Zirconia Stabilization-An X-ray Absorption Study: I, Trivalent Dopants. *Journal of the American Ceramic Society*, *77*(1), 118–128. https://doi.org/10.1111/j.1151-2916.1994.tb06964.x

Lutterotti, L. (2000). Maud: a Rietveld analysis program designed for the internet and experiment integration. *Acta Crystallographica Section a Foundations of Crystallography*, *56*(s1), s54–s54. https://doi.org/10.1107/s0108767300021954

M.P. Pechini, Method of preparing lead and alkaline earth titanates and niobates and coating method using the same to form a capacitor, US3330697 A, n.d.

Maček, J., Novosel, B., & Marinšek, M. (2007). Ni–YSZ SOFC anodes—Minimization of carbon deposition. *Journal of the European Ceramic Society*, *27*(2–3), 487–491. https://doi.org/10.1016/j.jeurceramsoc.2006.04.107

Matsui, T., Kishida, R., Muroyama, H., & Eguchi, K. (2012). Comparative Study on Performance Stability of Ni – Oxide Cermet Anodes under Humidified Atmospheres in Solid Oxide Fuel Cells, *159*(8), 456–460. https://doi.org/10.1149/2.053208jes

Mizutani, Y. (1995). Characterization of the Sc2O3-ZrO2 System and It's Application as the Electrolyte in Planar SOFC. *ECS Proceedings Volumes*, *1995–1*(1), 301–309. https://doi.org/10.1149/199501.0301pv

Sari, D., Piskin, F., Torunoglu, Z. C., Yasar, B., Kalay, Y. E., & Ozturk, T. (2018). Combinatorial development of nanocrystalline/amorphous (La,Sr)CoO3-(La,Sr)2CoO4 composite cathodes for IT-SOFCs. *Solid State Ionics*, *326*, 124–130. https://doi.org/10.1016/j.ssi.2018.10.003

Sase, M., Hermes, F., Yashiro, K., Sato, K., Mizusaki, J., Kawada, T., Sakai, N., & Yokokawa, H. (2008). Enhancement of Oxygen Surface Exchange at the Hetero-interface of (La,Sr)CoO[sub 3]/(La,Sr)[sub 2]CoO[sub 4] with PLD-Layered Films. *Journal of the Electrochemical Society*, *155*(8), B793. https://doi.org/10.1149/1.2928612

Shi, H., Su, C., Ran, R., Cao, J., & Shao, Z. (2020). Electrolyte materials for intermediate-temperature solid oxide fuel cells. *Progress in Natural Science: Materials International*, *30*(6), 764–774. https://doi.org/10.1016/j.pnsc.2020.09.003

Shijie, Z., Na, L., Liping, S., Qiang, L., Lihua, H., & Hui, Z. (2022). A novel high-entropy cathode with the A2BO4-type structure for solid oxide fuel cells.

Journal of Alloys and Compounds, *895*, 162548. https://doi.org/10.1016/j.jallcom.2021.162548

Simner, S., Bonnett, J., Canfield, N., Meinhardt, K., Shelton, J., Sprenkle, V., & Stevenson, J. (2003). Development of lanthanum ferrite SOFC cathodes. *Journal of Power Sources*, *113*(1), 1–10. https://doi.org/10.1016/s0378-7753(02)00455-x

Solovyev, A., Kuterbekov, K., Nurkenov, S., Nygymanova, A., Shipilova, A., Smolyanskiy, E., Rabotkin, S., & Ionov, I. (2021). Anode-supported solid oxide fuel cells with multilayer LSC/CGO/LSC cathode. *Fuel Cells*, *21*(4), 408–412. https://doi.org/10.1002/fuce.202000168

Spirin, A. V., Nikonov, A. V., Lipilin, A. S., Khrustov, V. R., Kuterbekov, K. A., Nurakhmetov, T. N., & Bekmyrza, K. Z. (2016). Effect of structural parameters of Ni-ScSZ cermet components on the SOFC anodes characteristics. *Russian Journal of Electrochemistry*, *52*(7), 613–621. https://doi.org/10.1134/s1023193516070181

Tao, J. (2013, May 1). *The Influence of Microstructure and Grain Boundary on the Electrical Properties of Scandia Stabilized Zirconia*. 2013 the Japan Institute of Metals and Materials. https://www.jstage.jst.go.jp/article/matertrans/54/5/54_M2012385/_article

Terki, R., Bertrand, G., Aourag, H., & Coddet, C. (2006). Structural and electronic properties of zirconia phases: A FP-LAPW investigations. *Materials Science in Semiconductor Processing*, *9*(6), 1006–1013. https://doi.org/10.1016/j.mssp.2006.10.033

Tsipis, E. V., & Kharton, V. V. (2008). Electrode materials and reaction mechanisms in solid oxide fuel cells: a brief review. *Journal of Solid State Electrochemistry*, *12*(11), 1367–1391. https://doi.org/10.1007/s10008-008-0611-6

Wackerl, J., Markus, T., Peck, D. H., Woo, S. K., & Singheiser, L. (2007). High-temperature Reactions between Scandia-doped Zirconia (ScSZ) and Cathode Materials. *ECS Transactions*, *7*(1), 859–867. https://doi.org/10.1149/1.2729176

Wang, Z., Qian, J., Wang, S., Cao, J., & Wen, T. (2008). Improvement of anode-supported solid oxide fuel cells. *Solid State Ionics*, *179*(27–32), 1593–1596. https://doi.org/10.1016/j.ssi.2008.03.022

Xu, Y., Xu, X., & Bi, L. (2022). A high-entropy spinel ceramic oxide as the cathode for proton-conducting solid oxide fuel cells. *Journal of Advanced Ceramics*, *11*(5), 794–804. https://doi.org/10.1007/s40145-022-0573-7

Yang, G., Su, C., Shi, H., Zhu, Y., Song, Y., Zhou, W., & Shao, Z. (2020). Toward Reducing the Operation Temperature of Solid Oxide Fuel Cells: Our Past 15 Years of Efforts in Cathode Development. *Energy &Amp; Fuels*, *34*(12), 15169–15194. https://doi.org/10.1021/acs.energyfuels.0c01887

Yang, Q., Wang, G., Wu, H., Beshiwork, B. A., Tian, D., Zhu, S., Yang, Y., Lu, X., Ding, Y., Ling, Y., Chen, Y., & Lin, B. (2021). A high-entropy perovskite cathode for solid oxide fuel cells. *Journal of Alloys and Compounds*, *872*, 159633. https://doi.org/10.1016/j.jallcom.2021.159633

Yeh, J. W., Chen, Y. L., Lin, S. J., & Chen, S. K. (2007). High-Entropy Alloys – A New Era of Exploitation. *Materials Science Forum*, *560*, 1–9. https://doi.org/10.4028/www.scientific.net/msf.560.1

Ye, Y., Wang, Q., Lu, J., Liu, C., & Yang, Y. (2016). High-entropy alloy: challenges and prospects. *Materials Today*, *19*(6), 349–362. https://doi.org/10.1016/j.mattod.2015.11.026

Zakaria, Z., Abu Hassan, S. H., Shaari, N., Yahaya, A. Z., & Boon Kar, Y. (2019). A review on recent status and challenges of yttria stabilized zirconia modification to lowering the temperature of solid oxide fuel cells operation. *International Journal of Energy Research*, *44*(2), 631–650. https://doi.org/10.1002/er.4944

Zhao, Q., Geng, S., Zhang, Y., Chen, G., Zhu, S., & Wang, F. (2022). High-entropy FeCoNiMnCu alloy coating on ferritic stainless steel for solid oxide fuel cell interconnects. *Journal of Alloys and Compounds*, *908*, 164608. https://doi.org/10.1016/j.jallcom.2022.164608

APPENDICES

A. Fabrication of LSF(rp) Sputter Target

So as to obtain LSF(p) sputter target, Ruddlesden-Popper type LSF powder, were pressed using deformable Teflon dies. Dies used had a 56 mm inner diameter with a 5 mm wall thickness with a height of 5 mm. The compaction was carried out at a pressure ranging from 64 MPa to 121 MPa. The compacts were then sintered at selected temperatures between 1300 to 1500°C. The treatment has however yielded a disc which was very fragile. Therefore, it was not possible to fabricate the disc in the solid form.

The sputter target, therefore was fabricated by pressing the powders into a copper holder, Fig A.1. The synthesized powder (LSF-rp) was filled into the holder and pressed at a pressure of 121 MPa using a closely matched punch. This has yielded a highly compacted powder in the form of disc housed in the copper holder.

Figure A.1. Copper holder used as a casing for sputter targets.

B. Fabrication of Anode (NiO-GDC)-Electrolyte (GDC) Bilayers

A bilayer comprising anode and electrolyte are often fabricated together onto which cathode is applied via a variety of means. In this section we first describe the fabrication of NiO-GDC anode-GDC electrolyte bilayer via tape casting and then we describe the fabrication of GDC electrolyte using sputter deposition technique.

B.1 GDC Electrolyte Layer Production by Tape Casting Method

GDC powder was synthesized using the Pechini method (M.P. Pechini, 1967). The weight fraction of nitrates used for this purpose are given in Table B.1. Here the fractions were chosen so as to yield powder with $Ce_{0.9}Gd_{0.1}O_{1.95}$ stoichiometry.

Table B.1. The fraction of nitrates used in the preparation of $Ce_{0.9}Gd_{0.1}O_{1.95}$ together with sol-gel additives.

	Gd Nitrate $Gd(NO_3)_3.6H_2O$	Ce Nitrate $Ce(NO_3)_3.6H_2O$	Citric acid	Ethylene Glycol
Molar Ratio	1	9	30	60
Weight Ratio	0.121 g	1.049	1.693	1

Dried gel was calcined at 850°C. XRD pattern of the resulting powder, i.e. GDC-10, is given in Fig. B.1(a). Rietveld refined pattern of the same powder is given in Fig. B.1(b).

Films were fabricated using alcohol-based tape casting method. The slurry preparation process is described in Figure B.2. The preparation was carried out in two stages. In the first stage, the main ceramic powders, solvents, and dispersant is mixed using a ball-milling process. In the second stage, binders and plasticizers are added to the slurry and ball-milled for the second time. Details of the ball milling are given in Fig. B.3. After ball milling, the slurry is mixed in a beaker for an additional 20 minutes so as to evaporate the excess alcohols. When the slurry thickens to dough

form, it is ready for tape casting. The blade was adjusted to 500 μm and the slurry was cast onto the glass substrate. After drying, the tape was removed from the glass and the discs of 18 mm diameter were obtained by punching the tape on a flat clean surface.

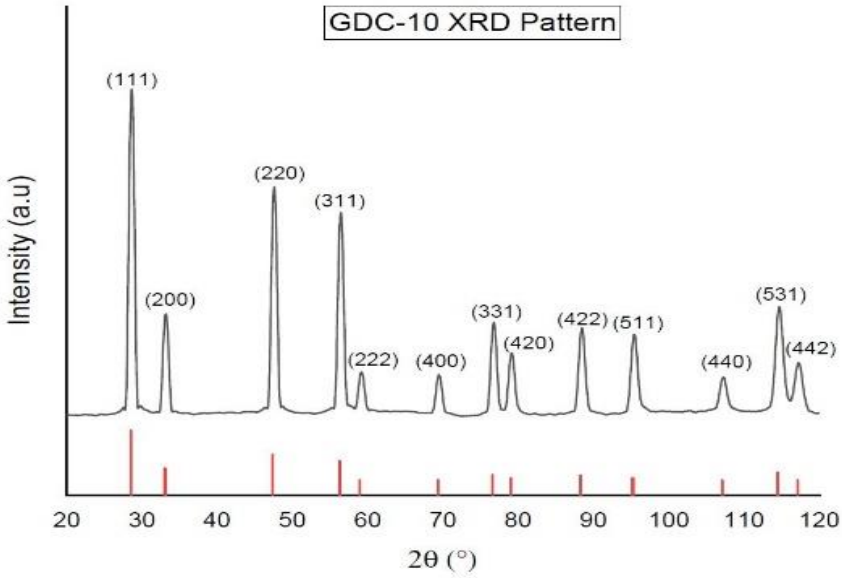

(a)

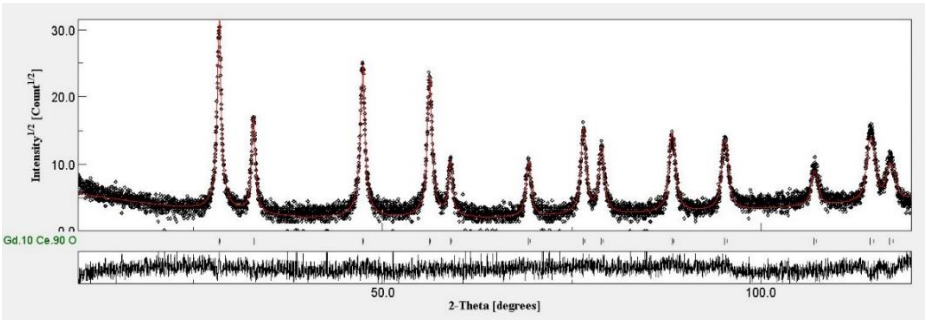

(b)

Figure B.1 GDC powder calcined at 850°C for 3 h. a) XRD pattern b) Rietveld refined XRD pattern.

Table B.2. Fraction of ingredients for preparation of electrolyte for the tape casting process.

Components (Function)	Weight Percent (%)	Weight (gm)
GDC (Ceramic Powder)	47	5.17
TEA (Dispersant)	2	0.22
Ethanol (Solvent)	21	2.31
MEK (Solvent)	21	2.31
PVB (Binder)	4.2	0.462
PEG (Plasticizer)	4.8	0.528
Whole Slurry	100	11

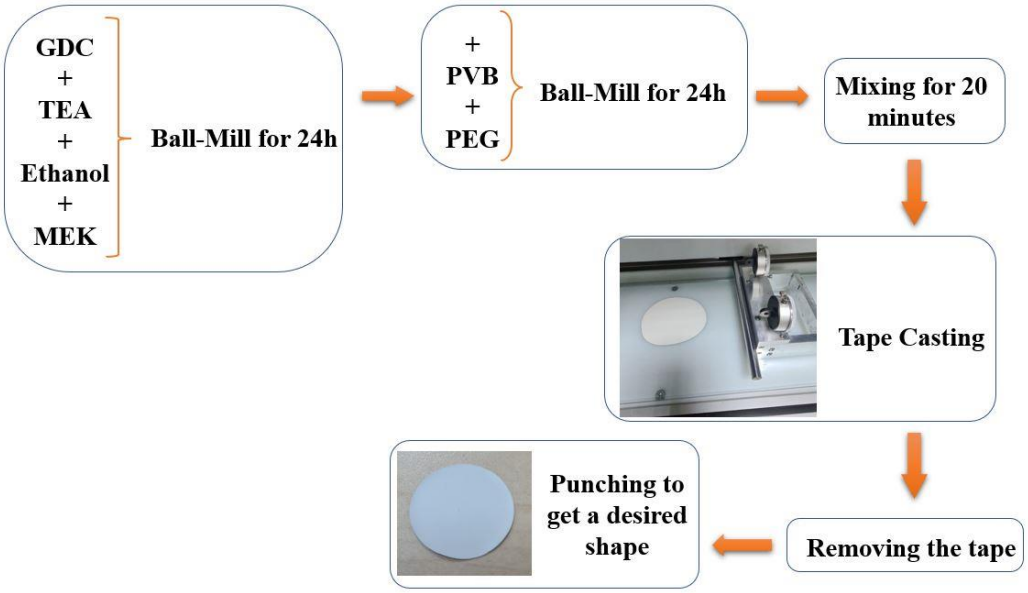

Figure B.2. Flowchart of electrolyte-making process for tape casting.

Figure B.3. Dried single electrolyte layer produced by tape casting technique.

B.2 NiO-GDC Anode Layer Fabrication by Tape casting Method

Anode layer was NiO-GDC. The fraction of chemicals used to prepare the slurry and the flow chart for processing are given in Table B.3 and Fig. B.4 respectively.

Table B.3. Composition of the prepared anode slurry for tape casting process.

Components (Function)	Weight Percent (%)	Weight (gm)
NiO (Ceramic Powder)	29.25	3.71
GDC (Ceramic Powder)	15.75	2
PVB (Binder)	4	0.508
PEG (Plasticizer)	4	0.508
TEA (Dispersant)	2	0.25
CB (Pore Former)	4.5	0.57
MEK (Solvent)	20.25	2.57
Ethanol (Solvent)	20.25	2.57
Whole Slurry	100	12.698

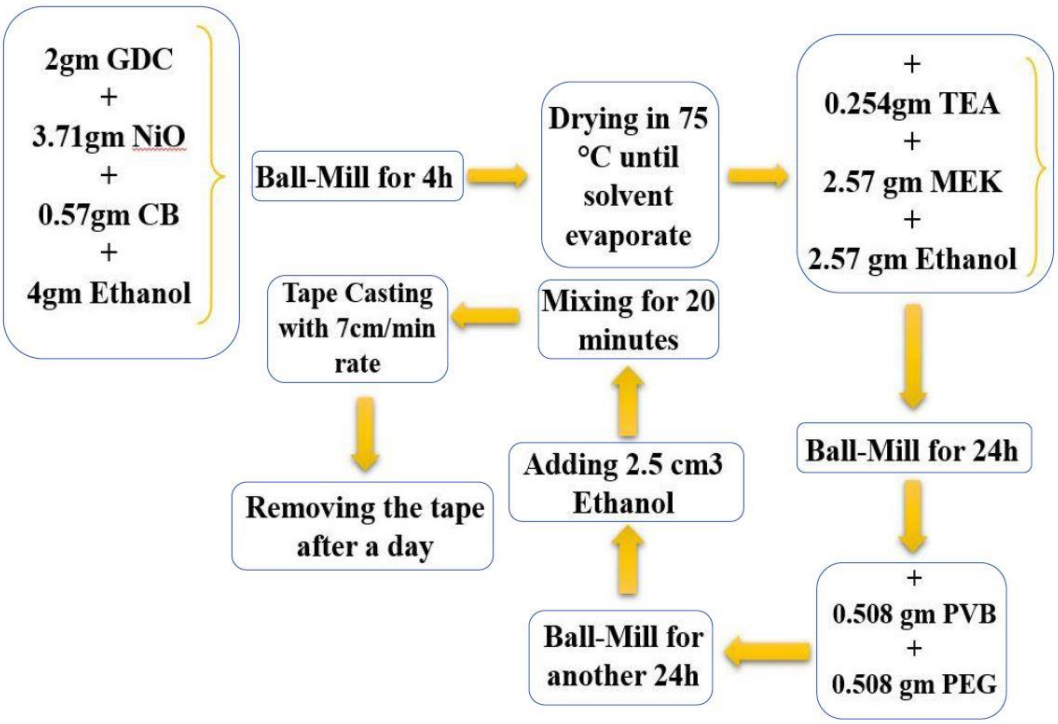

Figure B.4. Flowchart of anode-making process for tape casting.

Figure B.5. Dried anodes fabricated via tape casting.

The anode slurry was cast on the glass, the blade being adjusted to 500 μm, Fig. B.5. After drying which typically reduced the thickness to 200-250 μm, discs of 18 mm diameter were punched from the tape.

Typically, six discs were placed on top of one another. This was followed by an electrolyte disc which was placed at the top. The whole assembly were pressed under a pressure of 59 MPa. This has yielded a bilayer disc which were typically 620 μm thick, a greater fraction of which was anode.

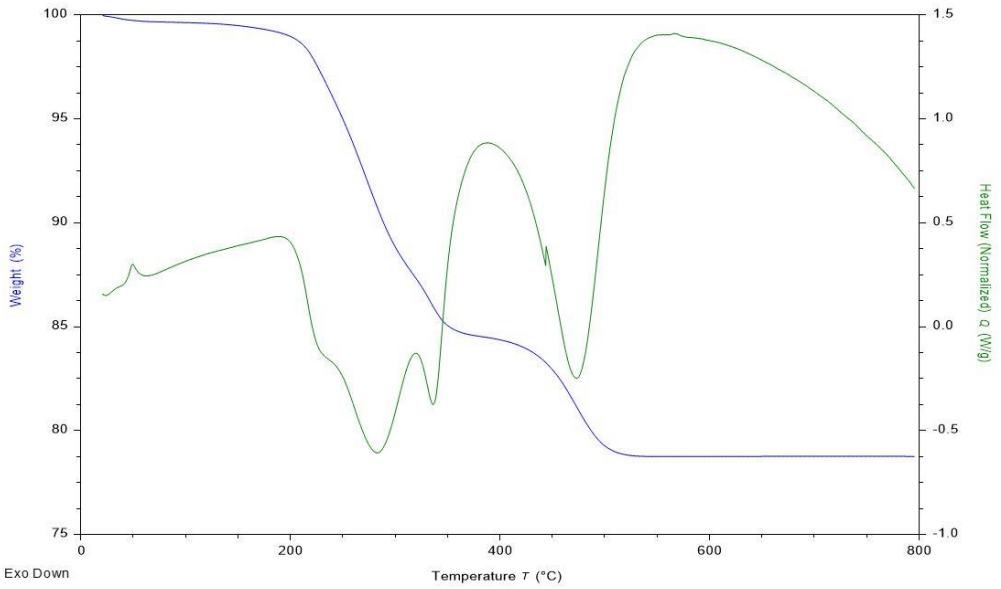

Figure B.6. Results of TGA thermal analysis of anode/electrolyte bilayer.

After preparing the single anode and electrolyte layers and pressing them on each other, co-sintering done in the furnace to have the final dense bilayers. However, due to the different thermal expansion coefficients of anode and electrolyte layers, in the co-sintering process, the most important challenge was the shrinkage of these layers or separation after sintering. The bilayer discs were then sintered at elevated temperatures. In order to determine the sintering regime, TGA measurement was taken up to 800°C, Fig B.6. As seen in Fig B.6. A decrease in mass starts from 50°C and accelerates after 200°C. The mass loss becomes less after 350^{o}C, and it is almost complete by 450°C. Based on this measurement, discs were heated at a rate of 0.5°C/min

up to 350°C where it was kept for an hour. Then it was continued heating with the same rate (0.5°C/min) up to 600°C. The heating rate was then increased to 1.5°C/min and continued up to 1350°C and maintained there for 2.5 hours. Discs were then cooled to room temperature at a rate of 1.5°C/min.

The best sintering route used by the mentioned techniques and the co-sintering process were done successfully, Fig B.7. (a) and (b). However, due to the reproducibility problems, it has been decided to change the method and use the magnetron sputter deposition technique to fabricate the electrolyte layer on the tape-casted anode layer substrates.

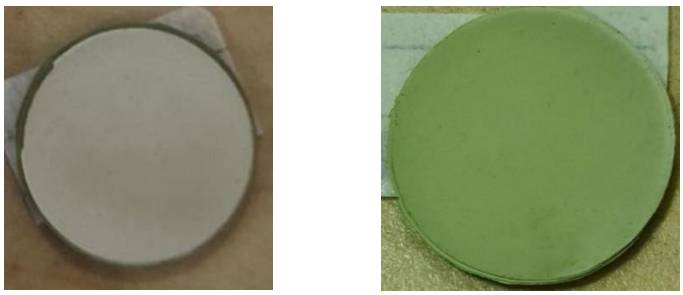

(a) (b)

Figure B.7. Sintered discs after tape casting (a) anode/electrolyte bilayer, (b) anode layer.

B.3 Sputter Deposition of GDC Electrolyte

Another method to fabricate bilayers is to use NiO-GDC anode layers as the substrate to deposit GDC electrolyte on them. To deposit the electrolyte layer on the anode, a circular sample holder was used, Fig. B.8. with 8rpm rotation.

Figure B.8. Placed anode layer after preparing by tape casting method on sample holder to do sputter deposition on them.

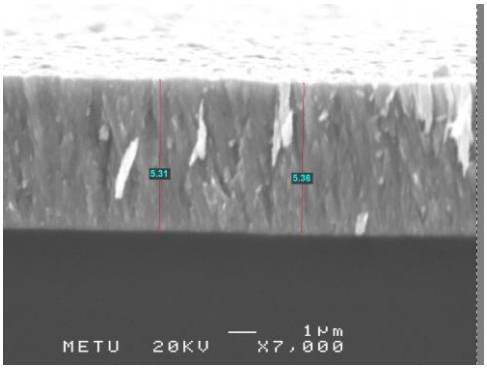

Figure B.9. SEM micrograph of electrolyte layer deposited by magnetron sputtering.

Figure B.10. Anode disc after sputter deposition of electrolyte layer on its surface.

Table B.4 Parameters used in sputter deposition of cathodes on the glass substrate.

Initial Pressure (Torr)	**Sputtering Pressure (mTorr)**	**Argon Flow Rate (sccm)**	**Oxygen Flow Rate (sccm)**
1.69×10^{-6}	5	20	5

Target	**Duration (h)**	**Rate (Å/s)**	**RF Power (Watt)**	**Measured SEM (µm)**
GDC	54	0.27	118	5.3

The parameters used for deposition are given in Table B.4. SEM micrograph of the deposited electrolyte is given in Fig.B.9. These anode-electrolyte bilayers (Fig.B.10) can be used to deposit cathodes on them so as further analyze the performance of the cathodes.